Cosmological Perturbations: Entering the Non-Linear Regime

Román Scoccimarro[1]
Department of Physics and Enrico Fermi Institute, University of Chicago, Chicago, IL 60637, and NASA/Fermilab Astrophysics Center, Fermi National Accelerator Laboratory, P.O.Box 500, Batavia, IL 60510

ABSTRACT

We consider one-loop corrections (non-linear corrections *beyond* leading order) to the bispectrum and skewness of cosmological density fluctuations induced by gravitational evolution, focusing on the case of Gaussian initial conditions and scale-free initial power spectra, $P(k) \propto k^n$. As has been established by comparison with numerical simulations, tree-level (leading order) perturbation theory describes these quantities at the largest scales. One-loop perturbation theory provides a tool to probe the transition to the non-linear regime on smaller scales. In this work, we find that, as a function of spectral index n, the one-loop bispectrum follows a pattern analogous to that of the one-loop power spectrum, which shows a change in behavior at a "critical index" $n_c \approx -1.4$, where non-linear corrections vanish. For the bispectrum, for $n \lesssim n_c$, one-loop corrections increase the configuration dependence of the leading order contribution; for $n \gtrsim n_c$, one-loop corrections tend to cancel the configuration dependence of the tree-level bispectrum, in agreement with known results from $n = -1$ numerical simulations. A similar situation is shown to hold for the Zel'dovich approximation, where $n_c \approx -1.75$. Using dimensional regularization, we obtain explicit analytic expressions for the one-loop bispectrum for $n = -2$ initial power spectra, for both the exact dynamics of gravitational instability and the Zel'dovich approximation. We also compute the skewness factor, including local averaging of the density field, for $n = -2$: $S_3(R) = 4.02 + 3.83\ \sigma_G^2(R)$ for gaussian smoothing and $S_3(R) = 3.86 + 3.18\ \sigma_{TH}^2(R)$ for top-hat smoothing, where $\sigma^2(R)$ is the variance of the density field fluctuations smoothed over a window of radius R. Comparison with fully non-linear numerical simulations implies that, for $n < -1$, one-loop perturbation theory can extend our understanding of nonlinear clustering down to scales where the transition to the stable clustering regime begins.

Subject headings: cosmology: large-scale structure of the universe

---

[1] *present address*: CITA, McLennan Physical Labs, 60 St George Street, Toronto, ON M5S 3H8.

1. Introduction

There is growing evidence that the large-scale structure of the Universe grew via gravitational instability from small primordial fluctuations in the matter density. For realistic models of structure formation, the initial spectrum of perturbations is such that at large scales, fluctuations are small and reflect the primordial spectrum. The variance of density fluctuations, $\sigma^2(R)$, is a decreasing function of scale R. At small scales, $\sigma^2(R)$ is large enough that non-linear effects become important. There are therefore two limiting regimes characterized by the value of $\sigma^2(R)$: the *linear regime* at large scales, where $\sigma^2(R) \ll 1$, and the *non-linear regime* at small scales, where $\sigma^2(R) \gg 1$. The boundary between these two regimes defines a length scale, the correlation length R_0, where $\sigma^2(R_0) = 1$. Because of gravitational instability, R_0 grows with time and therefore a given scale eventually becomes non-linear under time evolution.

At early epochs, the growth of density perturbations can be described by linear perturbation theory, provided that the linear power spectrum $P(k)$ falls off less steeply than k^4 for small k (Zel'dovich 1965, Peebles 1974, Peebles & Groth 1976). In the linear regime, perturbation Fourier modes evolve independently of one another, conserving the statistical properties of the primordial fluctuations. In particular, if the primordial fluctuations are Gaussian random fields, they remain Gaussian in linear theory. In this case, the statistical properties of the density and velocity fields are completely determined by the two-point correlation function or the power spectrum.

When the fluctuations become non-linear, coupling between different Fourier modes becomes important, inducing non-trivial correlations that modify the statistical properties of the cosmological fields. For Gaussian initial conditions, this causes the appearance of higher-order reduced correlations, which constitute independent statistics that can be measured in observational data and numerical simulations, even when the departure from the linear regime is small.

Non-linear cosmological perturbation theory provides a theoretical framework for the calculation of the induced higher-order correlation functions in the *weakly non-linear regime*, defined by scales R such that $\sigma(R) \lesssim 1$. At large scales, leading order (tree-level) perturbation theory gives the first non-vanishing contribution, and has been used to understand the generation of higher order correlations in gravitational instability. Comparison with fully non-linear numerical simulations has shown this approach to be very successful (Juszkiewicz, Bouchet & Colombi 1993, Bernardeau 1994b, Łokas et al. 1995, Gaztañaga & Baugh 1995, Baugh, Gaztañaga & Efstathiou 1995).

As one approaches smaller scales, however, next to leading order (loop) corrections

to the tree-level results are expected to become important. The question then arises of whether our understanding of non-linear clustering can be extended from the largest scales into the transition region to the non-linear regime. This motivates us to consider one-loop cosmological perturbation theory. In previous work (Scoccimarro & Frieman 1996b, hereafter SF2), we showed that for scale-free initial conditions, $P(k) \propto k^n$, without too much small-scale power (spectral index $n < -1$), one can understand the evolution of the power spectrum down to scales where it begins to go over to the strongly non-linear stable clustering regime. Therefore, it is interesting to consider one-loop corrections to the higher order correlation functions as well, to see if one can gain similar understanding of non-linear clustering on intermediate scales.

In this work we concentrate on one-loop corrections to the three-point function of density perturbations in Fourier space, also known as the bispectrum, and its one-point counterpart, the skewness. These are interesting quantities for several reasons. On the theoretical side, the bispectrum is the lowest order correlation function which, for Gaussian initial conditions, vanishes in the linear regime; its structure therefore reflects truly non-linear properties of the matter distribution. Furthermore, as the lowest order correlation function which depends on the vector character of its arguments, it gives direct physical information on the anisotropic structures and flows generated by gravitational instability. Observationally, the configuration dependence of the tree-level bispectrum has been put forward as a promising statistic to study the important but poorly understood issue of bias (Fry 1994), i.e., the degree to which luminous objects in the universe such as galaxies are fair tracers of the underlying density field. It is therefore important to see how further non-linear effects (which are inevitably present in observational studies) alter this configuration dependence, to check whether one can still disentangle nonlinear evolution from bias.

We focus on Gaussian initial conditions and scale-free initial power spectra, $P(k) \propto k^n$. In addition to mathematical simplicity, primordial Gaussian fluctuations have a broad physical motivation and are predicted by the simplest inflationary models. Although the linear power spectrum for the Universe is not scale-free (on both observational and theoretical grounds), scale-free spectra are very useful approximations over limited ranges of wavenumber k. They also have the advantage of yielding analytic closed form results and giving rise to self-similar evolution of the statistical properties of cosmological fields for spatially flat universes (Davis & Peebles 1977, Peebles 1980). In particular, self-similarity is a powerful aid towards a physical understanding of non-linear clustering and in many realistic models of structure formation we expect approximate self-similar evolution over a restricted range of length and time-scales (Efstathiou et al. 1988).

While the agreement between tree-level perturbation theory and numerical simulations

in the weakly non-linear regime is well established, it was not until recent years that N-body simulations have been able to reliably follow the transition of higher order statistics into the non-linear regime. In this regard, for scale-free initial power spectra, the bispectrum in numerical simulations has been shown by Fry, Melott & Shandarin (1993,1995) to depart from the tree-level perturbative results at scales comparable to the correlation length, as expected if next to leading order corrections are present. Similarly, for the skewness of the density field, and for higher-order cumulants as well, deviations from the leading order calculations have been reported in the literature (Bouchet & Hernquist 1992, Lucchin et al. 1994, Juszkiewicz et al. 1995, Hivon et al. 1995, Colombi, Bouchet & Hernquist 1996). We therefore consider it appropriate to extend the leading order calculations to one-loop, in order to understand better the limitations of the tree-level results and see the extent to which one can improve the agreement of perturbation theory with fully non-linear numerical simulations.

This paper is organized as follows. In Section 2 we discuss the cosmological fluid equations of motion and their solution within the framework of perturbation theory. For recent reviews of perturbation theory see Bernardeau (1996), Bouchet (1996), Juszkiewicz & Bouchet (1996); approximation methods in gravitational clustering are reviewed by Sahni & Coles (1996). Section 3 reviews the diagrammatic approach to perturbation theory and the self-similarity properties of statistical quantities derived from it. The main results of this work are presented in Section 4, where we consider for the first time one-loop corrections to the bispectrum and skewness including smoothing effects. We compare the latter with results from numerical simulations; a similar comparison for the bispectrum will be presented elsewhere (Scoccimarro et al 1996). Section 5 contains our conclusions. Auxiliary material is consider in the Appendices.

2. Dynamics and Perturbation Theory

2.1. Equations of Motion

The equations of motion relevant to gravitational instability describe conservation of mass and momentum and the Poisson equation for a self-gravitating perfect fluid with zero pressure in a homogeneous and isotropic universe (Peebles 1980):

$$\frac{\partial\delta(\mathbf{x},\tau)}{\partial\tau}+\nabla\cdot\{[1+\delta(\mathbf{x},\tau)]\mathbf{v}(\mathbf{x},\tau)\}=0, \tag{1}$$

$$\frac{\partial\mathbf{v}(\mathbf{x},\tau)}{\partial\tau}+\mathcal{H}(\tau)\ \mathbf{v}(\mathbf{x},\tau)+[\mathbf{v}(\mathbf{x},\tau)\cdot\nabla]\mathbf{v}(\mathbf{x},\tau)=-\nabla\Phi(\mathbf{x},\tau), \tag{2}$$

$$\nabla^2\Phi(\mathbf{x},\tau) = \frac{3}{2}\Omega\mathcal{H}^2(\tau)\delta(\mathbf{x},\tau) \tag{3}$$

Here, $\mathbf{x}$ denotes comoving spatial coordinates, $\tau = \int dt/a$ is the conformal time, $a(\tau)$ is the cosmic scale factor, the density contrast $\delta(\mathbf{x},\tau) \equiv \rho(\mathbf{x},\tau)/\bar{\rho} - 1$, with $\bar{\rho}(\tau)$ the mean density of matter, $\mathbf{v} \equiv d\mathbf{x}/d\tau$ represents the velocity field fluctuations about the Hubble flow, $\mathcal{H} \equiv d\ln a/d\tau = Ha$ is the conformal expansion rate, Φ is the gravitational potential due to the density fluctuations, and the density parameter $\Omega = \bar{\rho}/\rho_c = 8\pi G\bar{\rho}a^2/3\mathcal{H}^2$. We take the velocity field to be irrotational, so it can be completely described by its divergence $\theta \equiv \nabla\cdot\mathbf{v}$. We will refer to Eqs. (1)-(3) as the "exact dynamics" (ED), to make a distinction with the modified dynamics introduced by non-linear approximations such as the Zel'dovich approximation and the Local Lagrangian approximation to be discussed later (see Appendices B and C). Equations (1)-(3) hold in an arbitrary homogeneous and isotropic background Universe which evolves according to the Friedmann equations; henceforth, for simplicity we assume an Einstein-de Sitter background, $\Omega = 1$, with vanishing cosmological constant, for which $a \propto \tau^2$ and $3\Omega\mathcal{H}^2/2 = 6/\tau^2$.

Taking the divergence of Equation (2) and Fourier transforming the resulting equations of motion we get:

$$\frac{\partial\tilde{\delta}(\mathbf{k},\tau)}{\partial\tau} + \tilde{\theta}(\mathbf{k},\tau) = -\int d^3k_1 \int d^3k_2 \delta_D(\mathbf{k}-\mathbf{k}_1-\mathbf{k}_2)\alpha(\mathbf{k},\mathbf{k}_1)\tilde{\theta}(\mathbf{k}_1,\tau)\tilde{\delta}(\mathbf{k}_2,\tau), \tag{4}$$

$$\begin{aligned}\frac{\partial\tilde{\theta}(\mathbf{k},\tau)}{\partial\tau} &+ \mathcal{H}(\tau)\,\tilde{\theta}(\mathbf{k},\tau) + \frac{3}{2}\mathcal{H}^2(\tau)\tilde{\delta}(\mathbf{k},\tau) = \\ &- \int d^3k_1 \int d^3k_2 \delta_D(\mathbf{k}-\mathbf{k}_1-\mathbf{k}_2)\beta(\mathbf{k},\mathbf{k}_1,\mathbf{k}_2)\tilde{\theta}(\mathbf{k}_1,\tau)\tilde{\theta}(\mathbf{k}_2,\tau),\end{aligned} \tag{5}$$

(δ_D denotes the three-dimensional Dirac delta distribution), where the functions

$$\alpha(\mathbf{k},\mathbf{k}_1) \equiv \frac{\mathbf{k}\cdot\mathbf{k}_1}{k_1^2}, \qquad \beta(\mathbf{k},\mathbf{k}_1,\mathbf{k}_2) \equiv \frac{k^2(\mathbf{k}_1\cdot\mathbf{k}_2)}{2k_1^2k_2^2} \tag{6}$$

encode the non-linearity of the evolution (mode coupling) and come from the non-linear terms in the continuity equation (1) and the Euler equation (2) respectively.

2.2. Perturbation Theory Solutions

We focus on a statistical description of cosmological perturbations: we are interested in correlation functions of the fields $\tilde{\delta}(\mathbf{k},\tau)$ and $\tilde{\theta}(\mathbf{k},\tau)$ (i.e., the ensemble average of products

of these fields). Ensemble averaging effectively introduces a new parameter into the problem, the variance of the density fluctuations $\sigma^2 \equiv < \delta^2 >$, which controls the transition from the linear ($\sigma^2 \ll 1$) to the non-linear regime ($\sigma^2 \gg 1$). We consider perturbations about the linear solution, effectively treating the variance of the linear fluctuations as a small parameter. In this case, Eqs. (4)-(5) can be formally solved via a perturbative expansion,

$$\tilde{\delta}(\mathbf{k},\tau) = \sum_{n=1}^{\infty} a^n(\tau)\delta_n(\mathbf{k}), \qquad \tilde{\theta}(\mathbf{k},\tau) = \mathcal{H}(\tau)\sum_{n=1}^{\infty} a^n(\tau)\theta_n(\mathbf{k}), \tag{7}$$

where only the fastest growing mode at each order is taken into account. At small a, the series are dominated by their first terms, and since $\theta_1(\mathbf{k}) = -\delta_1(\mathbf{k})$ from the continuity equation, $\delta_1(\mathbf{k})$ completely characterizes the linear fluctuations. The equations of motion (4)-(5) determine $\delta_n(\mathbf{k})$ and $\theta_n(\mathbf{k})$ in terms of the linear fluctuations,

$$\delta_n(\mathbf{k}) = \int d^3q_1 \ldots \int d^3q_n \delta_D(\mathbf{k}-\mathbf{q}_1-\ldots-\mathbf{q}_n) F_n^{(s)}(\mathbf{q}_1,\ldots,\mathbf{q}_n)\delta_1(\mathbf{q}_1)\ldots\delta_1(\mathbf{q}_n), \tag{8}$$

$$\theta_n(\mathbf{k}) = -\int d^3q_1 \ldots \int d^3q_n \delta_D(\mathbf{k}-\mathbf{q}_1-\ldots-\mathbf{q}_n) G_n^{(s)}(\mathbf{q}_1,\ldots,\mathbf{q}_n)\delta_1(\mathbf{q}_1)\ldots\delta_1(\mathbf{q}_n), \tag{9}$$

where $F_n^{(s)}$ and $G_n^{(s)}$ are symmetric homogeneous functions with degree zero of the wave vectors $\{\mathbf{q}_1,\ldots,\mathbf{q}_n\}$. They are constructed from the fundamental mode coupling functions $\alpha(\mathbf{k},\mathbf{k}_1)$ and $\beta(\mathbf{k},\mathbf{k}_1,\mathbf{k}_2)$ according to the recursion relations ($n \geq 2$, see Goroff et al. (1986) or Jain & Bertschinger (1994) for a derivation):

$$\begin{aligned} F_n(\mathbf{q}_1,\ldots,\mathbf{q}_n) &= \sum_{m=1}^{n-1} \frac{G_m(\mathbf{q}_1,\ldots,\mathbf{q}_m)}{(2n+3)(n-1)}\Big[(2n+1)\alpha(\mathbf{k},\mathbf{k}_1)F_{n-m}(\mathbf{q}_{m+1},\ldots,\mathbf{q}_n) \\ &+ 2\beta(\mathbf{k},\mathbf{k}_1,\mathbf{k}_2)G_{n-m}(\mathbf{q}_{m+1},\ldots,\mathbf{q}_n)\Big], \end{aligned} \tag{10}$$

$$\begin{aligned} G_n(\mathbf{q}_1,\ldots,\mathbf{q}_n) &= \sum_{m=1}^{n-1} \frac{G_m(\mathbf{q}_1,\ldots,\mathbf{q}_m)}{(2n+3)(n-1)}\Big[3\alpha(\mathbf{k},\mathbf{k}_1)F_{n-m}(\mathbf{q}_{m+1},\ldots,\mathbf{q}_n) \\ &+ 2n\beta(\mathbf{k},\mathbf{k}_1,\mathbf{k}_2)G_{n-m}(\mathbf{q}_{m+1},\ldots,\mathbf{q}_n)\Big], \end{aligned} \tag{11}$$

(where $\mathbf{k}_1 \equiv \mathbf{q}_1 + \ldots + \mathbf{q}_m$, $\mathbf{k}_2 \equiv \mathbf{q}_{m+1} + \ldots + \mathbf{q}_n$, $\mathbf{k} \equiv \mathbf{k}_1 + \mathbf{k}_2$, and $F_1 = G_1 \equiv 1$) and the symmetrization procedure:

$$F_n^{(s)}(\mathbf{q}_1,\ldots,\mathbf{q}_n) = \frac{1}{n!}\sum_{\pi} F_n(\mathbf{q}_{\pi(1)},\ldots,\mathbf{q}_{\pi(n)}), \tag{12}$$

$$G_n^{(s)}(\mathbf{q}_1,\ldots,\mathbf{q}_n) = \frac{1}{n!}\sum_{\pi} G_n(\mathbf{q}_{\pi(1)},\ldots,\mathbf{q}_{\pi(n)}), \tag{13}$$

where the sum is taken over all the permutations π of the set $\{1,\ldots,n\}$.

3. Statistics and Diagrammatics

3.1. Diagrammatic Expansion of Statistical Quantities

The starting point for a statistical description of fluctuations in cosmology is the "Fair Sample Hypothesis" (Peebles 1980, Bertschinger 1992). This asserts that fluctuations can be described by statistically homogeneous and isotropic random fields (so that our Universe is a random realization from a statistical ensemble) and that within the accessible part of the Universe there are many independent samples that can be considered to approximate a statistical ensemble, so that spatial averages are equivalent to ensemble averages ("ergodicity"). In this work we focus on the non-linear evolution of the three-point cumulant of the density field, the bispectrum $B(\mathbf{k}_1,\mathbf{k}_2,\tau)$, and its 1-point counterpart, the skewness factor $S_3(R,\tau)$. These are defined respectively by:

$$\left\langle \tilde{\delta}(\mathbf{k}_1,\tau)\tilde{\delta}(\mathbf{k}_2,\tau)\tilde{\delta}(\mathbf{k}_3,\tau)\right\rangle_c = \delta_D(\mathbf{k}_1+\mathbf{k}_2+\mathbf{k}_3)\ B(\mathbf{k}_1,\mathbf{k}_2,\tau), \tag{14}$$

and

$$S_3(R,\tau) = \frac{1}{\sigma^4(R,\tau)}\int B(\mathbf{k}_1,\mathbf{k}_2,\tau)\ W(k_1R)W(k_2R)W(|\mathbf{k}_1+\mathbf{k}_2|R)\ d^3k_1 d^3k_2, \tag{15}$$

where the angle brackets denote ensemble averaging , the subscript "c" stands for the connected contribution (see below), and $\sigma^2(R,\tau)$ is the variance of the density field fluctuations:

$$\sigma^2(R,\tau) = \int P(k,\tau)\ W^2(kR)\ d^3k = \left\langle \delta^2(R,\tau)\right\rangle. \tag{16}$$

Here the power spectrum $P(k,\tau)$ is defined by

$$\left\langle \tilde{\delta}(\mathbf{k},\tau)\tilde{\delta}(\mathbf{k}',\tau)\right\rangle_c = \delta_D(\mathbf{k}+\mathbf{k}')P(k,\tau), \tag{17}$$

and therefore

$$S_3(R,\tau) = \frac{\left\langle \delta^3(R,\tau)\right\rangle_c}{\left\langle \delta^2(R,\tau)\right\rangle^2}. \tag{18}$$

Here $W(kR)$ is the Fourier transform of the window function, which we take to be either a top-hat (TH) or a Gaussian (G),

$$W_{\rm TH}(u) = \frac{3}{u^3}\Big[\sin(u) - u\cos(u)\Big], \tag{19}$$

$$W_{\rm G}(u) = \exp(-u^2/2). \tag{20}$$

It is convenient to define the hierarchical amplitude Q as follows (Fry & Seldner 1982, Fry 1984):

$$Q \equiv \frac{B(\mathbf{k}_1,\mathbf{k}_2,\tau)}{P(k_1,\tau)P(k_2,\tau) + P(k_2,\tau)P(k_3,\tau) + P(k_3,\tau)P(k_1,\tau)}, \tag{21}$$

which has the desirable property that it is scale and time independent to lowest order (tree-level) in non-linear perturbation theory. In a pure hierarchical model, Q would be a fixed constant, independent of configuration and of the power spectrum $P(k,\tau)$ as well.

We are interested in calculating the non-linear evolution of these statistical quantities from Gaussian initial conditions in the weakly non-linear regime, $\sigma(R) \lesssim 1$. A systematic framework for calculating correlations of cosmological fields in perturbation theory has been formulated using diagrammatic techniques (Goroff et al. 1986, Wise 1988, Scoccimarro & Frieman 1996 (SF1) , SF2). In this approach, contributions to p-point cumulants of the density field come from connected diagrams with p external (solid) lines and $r = p-1, p, \ldots$ internal (dashed) lines. The perturbation expansion leads to a collection of diagrams at each order, the leading order being tree-diagrams, the next to leading order 1-loop diagrams and so on. In each diagram, external lines represent the spectral components of the fields we are interested in (e.g., $\delta(\mathbf{k},\tau)$). Each internal line is labeled by a wave-vector that is integrated over, and represents a linear power spectrum $P_{11}(q,\tau)$. Vertices of order n (i.e., where n internal lines join) represent an $n^{\rm th}$ order perturbative solution δ_n, and momentum conservation is imposed at each vertex.

We can write the loop expansion for the power spectrum up to one-loop corrections as

$$P(k,\tau) = P^{(0)}(k,\tau) + P^{(1)}(k,\tau) + \ldots, \tag{22}$$

where the superscript (n) denotes an n-loop contribution, the tree-level (0-loop) contribution is just the linear spectrum,

$$P^{(0)}(k,\tau) = P_{11}(k,\tau), \tag{23}$$

with $a^2(\tau)\langle\delta_1(\mathbf{k})\delta_1(\mathbf{k}')\rangle_c = \delta_D(\mathbf{k}+\mathbf{k}')P_{11}(k,\tau)$, and the 1-loop contribution consists of two terms,

$$P^{(1)}(k,\tau) = P_{22}(k,\tau) + P_{13}(k,\tau), \tag{24}$$

with (see Fig. 1):

$$P_{22}(k,\tau) \equiv 2\int [F_2^{(s)}(\mathbf{k}-\mathbf{q},\mathbf{q})]^2 P_{11}(|\mathbf{k}-\mathbf{q}|,\tau)P_{11}(q,\tau)d^3q, \tag{25}$$

$$P_{13}(k,\tau) \equiv 6\int F_3^{(s)}(\mathbf{k},\mathbf{q},-\mathbf{q})P_{11}(k,\tau)P_{11}(q,\tau)d^3q. \tag{26}$$

Here P_{ij} denotes the amplitude given by the above rules for a connected diagram representing the contribution from $\langle\delta_i\delta_j\rangle_c$ to the power spectrum. We have assumed Gaussian initial conditions, for which P_{ij} vanishes if $i+j$ is odd.

For the smoothed variance we write

$$\sigma^2(R) = \sigma_\ell^2(R)\Big(1 + s^{(1)}\ \sigma_\ell^2(R) + \dots\Big), \tag{27}$$

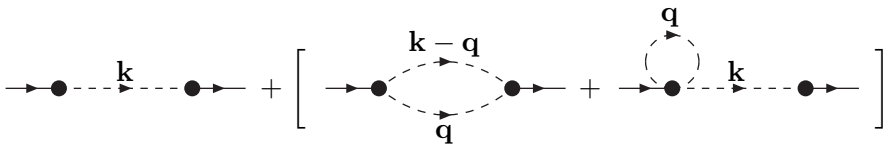

(P_{11}) (P_{22}) (P_{13})

Fig. 1.— Diagrams for the power spectrum up to one-loop. See Eqs. (25) and (26) for diagram amplitudes.

where $\sigma_\ell^2(R)$ denotes the variance in linear theory (given by (16) with $P = P_{11}$); the dimensionless 1-loop amplitude is

$$s^{(1)}(R) \equiv \frac{1}{\sigma_\ell^4(R)} \int P^{(1)}(k,\tau)\ W^2(kR)\ d^3k. \tag{28}$$

To characterize the degree of non-linear evolution when including one-loop corrections to the power spectrum and bispectrum, it is convenient to define a physical scale from the linear power spectrum, the correlation length R_0, as the scale where the smoothed linear variance is unity,

$$\sigma_\ell^2(R_0) = \int d^3k\ P_{11}(k,\tau)\ W^2(kR_0) \equiv 1. \tag{29}$$

The loop expansion for the bispectrum reads:

$$B(\mathbf{k}_1,\mathbf{k}_2,\tau) = B^{(0)}(\mathbf{k}_1,\mathbf{k}_2,\tau) + B^{(1)}(\mathbf{k}_1,\mathbf{k}_2,\tau) + \ldots, \tag{30}$$

where the tree-level part is given by a single diagram in second order perturbation theory (see Fig. 2) plus its permutations over external momenta (recall that $\mathbf{k}_1 + \mathbf{k}_2 + \mathbf{k}_3 \equiv 0$):

$$\begin{aligned} B^{(0)}(\mathbf{k}_1,\mathbf{k}_2,\tau) \ &\equiv\ 2P_{11}(k_1,\tau)P_{11}(k_2,\tau)F_2^{(s)}(\mathbf{k}_1,\mathbf{k}_2) + 2P_{11}(k_2,\tau)P_{11}(k_3,\tau) \\ &\quad \times F_2^{(s)}(\mathbf{k}_2,\mathbf{k}_3) + 2P_{11}(k_3,\tau)P_{11}(k_1,\tau)F_2^{(s)}(\mathbf{k}_3,\mathbf{k}_1). \end{aligned} \tag{31}$$

The one-loop contribution consists of four distinct diagrams involving up to fourth-order solutions:

$$B^{(1)}(\mathbf{k}_1,\mathbf{k}_2,\tau) \equiv B_{222}(\mathbf{k}_1,\mathbf{k}_2,\tau) + B^I_{321}(\mathbf{k}_1,\mathbf{k}_2,\tau) + B^{II}_{321}(\mathbf{k}_1,\mathbf{k}_2,\tau) + B_{411}(\mathbf{k}_1,\mathbf{k}_2,\tau), \tag{32}$$

where:

$$\begin{aligned} B_{222} \ &\equiv\ 8\int d^3q P_{11}(q,\tau)F_2^{(s)}(-\mathbf{q},\mathbf{q}+\mathbf{k}_1)P_{11}(|\mathbf{q}+\mathbf{k}_1|,\tau)F_2^{(s)}(-\mathbf{q}-\mathbf{k}_1,\mathbf{q}-\mathbf{k}_2) \\ &\quad \times P_{11}(|\mathbf{q}-\mathbf{k}_2|,\tau)F_2^{(s)}(\mathbf{k}_2-\mathbf{q},\mathbf{q}), \\ B^I_{321} \ &\equiv\ 6P_{11}(k_3,\tau)\int d^3q P_{11}(q,\tau)F_3^{(s)}(-\mathbf{q},\mathbf{q}-\mathbf{k}_2,-\mathbf{k}_3)P_{11}(|\mathbf{q}-\mathbf{k}_2|,\tau) \end{aligned} \tag{33}$$

$$\times F_2^{(s)}(\mathbf{q}, \mathbf{k}_2 - \mathbf{q}) + \text{permutations}, \tag{34}$$

$$B_{321}^{II} \equiv 6P_{11}(k_2,\tau)P_{11}(k_3,\tau)F_2^{(s)}(\mathbf{k}_2,\mathbf{k}_3)\int d^3qP_{11}(q,\tau)F_3^{(s)}(\mathbf{k}_3,\mathbf{q},-\mathbf{q}) + \text{permutations}, \tag{35}$$

$$B_{411} \equiv 12P_{11}(k_2,\tau)P_{11}(k_3,\tau)\int d^3qP_{11}(q,\tau)F_4^{(s)}(\mathbf{q},-\mathbf{q},-\mathbf{k}_2,-\mathbf{k}_3) + \text{permutations}. \tag{36}$$

For the hierarchical amplitude Q (see Eq. (21)), the loop expansion yields:

$$Q \equiv \frac{B^{(0)}(\mathbf{k}_1,\mathbf{k}_2,\tau) + B^{(1)}(\mathbf{k}_1,\mathbf{k}_2,\tau) + \ldots}{\Sigma^{(0)}(\mathbf{k}_1,\mathbf{k}_2,\tau) + \Sigma^{(1)}(\mathbf{k}_1,\mathbf{k}_2,\tau) + \ldots}, \tag{37}$$

where:

$$\Sigma^{(0)}(\mathbf{k}_1,\mathbf{k}_2,\tau) \equiv P_{11}(k_1,\tau)P_{11}(k_2,\tau) + P_{11}(k_2,\tau)P_{11}(k_3,\tau) + P_{11}(k_3,\tau)P_{11}(k_1,\tau), \tag{38}$$

and:

$$\Sigma^{(1)}(\mathbf{k}_1,\mathbf{k}_2,\tau) \equiv P^{(0)}(k_1,\tau)P^{(1)}(k_2,\tau) + \text{permutations}. \tag{39}$$

For large scales, it is possible to expand $Q \equiv Q^{(0)} + Q^{(1)} + \ \ldots$, which gives:

$$Q^{(0)} \equiv \frac{B^{(0)}(\mathbf{k}_1,\mathbf{k}_2,\tau)}{\Sigma^{(0)}(\mathbf{k}_1,\mathbf{k}_2,\tau)}, \tag{40}$$

$$Q^{(1)} \equiv \frac{B^{(1)}(\mathbf{k}_1,\mathbf{k}_2,\tau) - Q^{(0)}\Sigma^{(1)}(\mathbf{k}_1,\mathbf{k}_2,\tau)}{\Sigma^{(0)}(\mathbf{k}_1,\mathbf{k}_2,\tau)} \equiv \tilde{Q}^{(1)} - Q^{(0)}\ \frac{\Sigma^{(1)}(\mathbf{k}_1,\mathbf{k}_2,\tau)}{\Sigma^{(0)}(\mathbf{k}_1,\mathbf{k}_2,\tau)}. \tag{41}$$

Note that $Q^{(1)}$ depends on the normalization of the linear power spectrum, and its amplitude increases with time evolution. On the other hand, from Equations (31) and (40) it follows that $Q^{(0)}$ is independent of time and normalization (Fry 1984). Furthermore, for scale-free initial conditions, $P_{11}(k) \propto k^n$, $Q^{(0)}$ is also independent of overall scale. For the particular case of equilateral configurations ($k_1 = k_2 = k_3$ and $\hat{k}_i \cdot \hat{k}_j = -0.5$ for all pairs), $Q^{(0)}$ is independent of spectral index as well, $Q^{(0)}_{EQ} = 4/7$. In general, for scale-free initial power spectra, $Q^{(0)}$ depends on configuration shape through, e.g., the ratio k_1/k_2 and the angle θ defined by $\hat{k}_1 \cdot \hat{k}_2 = \cos\theta$. Note that we also defined $\tilde{Q}^{(1)}$ in Eq. (41) which denotes the

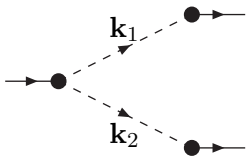

(B_{211})

Fig. 2.— Tree-level diagram for the bispectrum. This diagram plus its 2 permutations over external momenta generates the tree-level bispectrum. The corresponding amplitudes are given by Eq. (31).

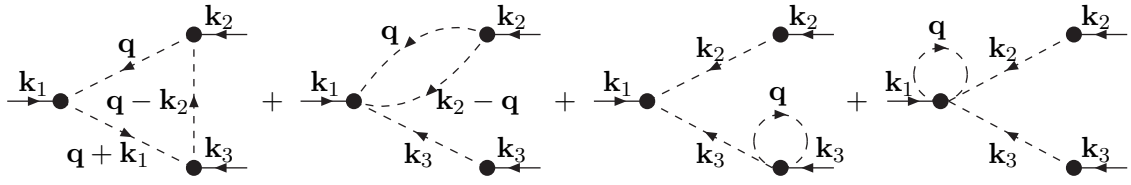

(B_{222}) (B^I_{321}) (B^{II}_{321}) (B_{411})

Fig. 3.— One-loop diagrams for the bispectrum. The corresponding amplitudes are given in Eqs. (33) through (36).

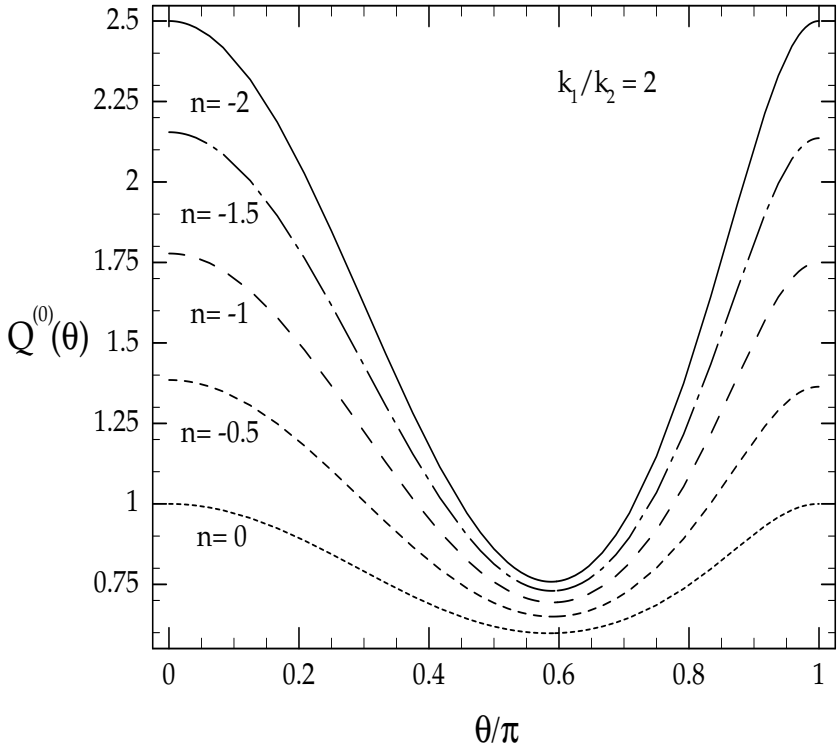

Fig. 4.— The tree-level hierarchical amplitude $Q^{(0)}$ for triangle configurations given by $k_1/k_2 = 2$ as a function of the angle θ ($\hat{k}_1 \cdot \hat{k}_2 = \cos\theta$). The different curves correspond to spectral indices $n = -2, -1.5, -1, -0.5, 0$ (from top to bottom). See also Fry (1994)

one-loop correction to the bispectrum normalized by the tree-level quantity $\Sigma^{(0)}$; this will be useful in order to assess the behavior of the one-loop bispectrum with spectral index.

Figure 4 shows $Q^{(0)}$ for the triangle configuration given by $k_1/k_2 = 2$ as a function of θ for different spectral indices. The configuration dependence of $Q^{(0)}$ is remarkably insensitive to other cosmological parameters, such as the density parameter Ω and the cosmological constant (Fry 1994) (see also Hivon et al. (1995)). In fact, since bias between the galaxies and the underlying density field is known to change this configuration dependence (Fry & Gaztañaga 1993), measurements of the hierarchical amplitude Q in galaxy surveys could provide a measure of bias which is insensitive to other poorly known cosmological parameters (Fry 1994), unlike the usual determination from peculiar velocities which has a degeneracy with the density parameter Ω.

The configuration dependence of $Q^{(0)}$ comes from the second order perturbation theory kernel $F_2^{(s)}$ (see Eqs. (40) and (31)) and can be understood in physical terms as follows. From the recursion relations given in Eq. (10), we can write:

$$F_2^{(s)}(\mathbf{k}_1,\mathbf{k}_2) = \frac{5}{14}\,\Big[\alpha(\mathbf{k},\mathbf{k}_1)+\alpha(\mathbf{k},\mathbf{k}_2)\Big] + \frac{2}{7}\,\beta(\mathbf{k},\mathbf{k}_1,\mathbf{k}_2), \tag{42}$$

where $\mathbf{k}\equiv\mathbf{k}_1+\mathbf{k}_2$ (see Eq. (6) for definitions of the mode-coupling functions α and β). The terms in square brackets contribute a constant term, independent of configuration, coming from the $\theta\times\delta$ term in the equations of motion, plus terms which depend on configuration and describe gradients of the density field in the direction of the flow (i.e., the term $\mathbf{v}\cdot\nabla\delta$ in the continuity equation). Similarly, the last term in Eq. (42) contributes configuration dependent terms which come from gradients of the velocity divergence in the direction of the flow (due to the term $(\mathbf{v}\cdot\nabla)\mathbf{v}$ in Euler's equation). Therefore, the configuration dependence of the bispectrum reflects the anisotropy of structures and flows generated by gravitational instability. The enhancement of correlations for collinear wavevectors ($\theta=0,\pi$) in Figure 4, reflects the fact that gravitational instability generates density and velocity divergence gradients which are mostly parallel to the flow. Upon ensemble averaging, which by ergodicity corresponds to weighting configurations by their number frequency, this leads to a predominance of correlations in nearly collinear configurations. The dependence on the spectrum is also easy to understand: models with more large-scale power (smaller spectral indices n) give rise to anisotropic structures and flows with larger coherence length, which upon ensemble averaging leads to a more anisotropic bispectrum. We will see in the next Section that this physical picture provides some insight into the behavior of one-loop corrections.

The loop expansion for the skewness factor gives (SF1):

$$S_3(R) \equiv \frac{S_3^{(0)} + \tilde{S}_3^{(1)}\sigma^2(R) + \ldots}{1 + 2s^{(1)}\sigma^2(R) + \ldots}, \tag{43}$$

where:

$$S_3^{(0)}(R) \equiv \frac{1}{\sigma_\ell^4(R)} \int d^3k_1 d^3k_2 B^{(0)}(\mathbf{k}_1,\mathbf{k}_2)\; W(k_1R)W(k_2R)W(|\mathbf{k}_1+\mathbf{k}_2|R), \tag{44}$$

$$\tilde{S}_3^{(1)}(R) \equiv \frac{1}{\sigma_\ell^6(R)} \int d^3k_1 d^3k_2 B^{(1)}(\mathbf{k}_1,\mathbf{k}_2)\; W(k_1R)W(k_2R)W(|\mathbf{k}_1+\mathbf{k}_2|R). \tag{45}$$

For large scales, the expansion in Eq. (43) can be rewritten as $S_3 \equiv S_3^{(0)} + S_3^{(1)}\sigma^2 + \ldots$, where:

$$S_3^{(1)}(R) \equiv \tilde{S}_3^{(1)}(R) - 2\; s^{(1)}(R)\; S_3^{(0)}(R). \tag{46}$$

The tree-level skewness has been thoroughly studied (Goroff et al. 1986, Juszkiewicz et al. 1993, Bernardeau 1992, Bernardeau 1994, Łokas et al. 1995) including smoothing effects for both top-hat and Gaussian smoothing. The result for scale-free initial power spectra is:

$$S_3^{(0)} = \frac{34}{7} - (n+3), \tag{47}$$

for top-hat smoothing (Bernardeau 1992b, Juszkiewicz et al. 1993), and:

$$S_3^{(0)} = 3\ {}_2\mathrm{F}_1\Big(\frac{n+3}{2}, \frac{n+3}{2}, \frac{3}{2}, \frac{1}{4}\Big) - \Big(n + \frac{8}{7}\Big)\ {}_2\mathrm{F}_1\Big(\frac{n+3}{2}, \frac{n+3}{2}, \frac{5}{2}, \frac{1}{4}\Big), \tag{48}$$

for Gaussian smoothing (Łokas et al. 1995, Matsubara 1994), where ${}_2\mathrm{F}_1$ denotes a hypergeometric function. More specifically, $S_3^{(0)} = 4.02,\ 3.71,\ 3.47,\ 3.28,\ 3.14$ for $n = -2, -1.5, -1, -0.5, 0$ for Gaussian smoothing. See Appendix B for the corresponding results in the Zel'dovich approximation.

3.2. Self-Similarity and Perturbation Theory

Since there is no preferred scale in the dynamics of a self-gravitating pressureless perfect fluid in an Einstein-de Sitter universe, Eqs. (1)-(3) admit self-similar solutions (Peebles 1980). This means that correlation functions of the cosmological fields should scale with a self-similarity variable, given appropriate initial conditions: knowing a statistical quantity at a given time completely specifies its evolution. For Gaussian initial conditions and scale-free power spectra, one can define a physical scale R_0, the correlation length (see Eq. (29)), which obeys $R_0 \propto a^{2/(n+3)}$ in linear theory (and in general if the non-linear power spectrum evolves self-similarly). Statistical quantities in linear perturbation theory evolve self-similarly with R_0, e.g.,

$$R_0^{-3} P^{(0)}(k,\tau) \equiv \mathcal{P}^{(0)}(kR_0), \tag{49}$$

$$R_0^{-6} B^{(0)}(\mathbf{k}_1, \mathbf{k}_2, \tau) \equiv \mathcal{B}^{(0)}(\mathbf{k}_1 R_0, \mathbf{k}_2 R_0). \tag{50}$$

When loop corrections are taken into account, however, self-similarity may be broken by the appearance of new scales required by infrared and ultraviolet divergences in the loop integrations. In fact, one may consider a linear power spectrum $P_{11}(k,\tau)$ given by a truncated power-law,

$$P_{11}(k,\tau) \equiv \begin{cases} A\ a^2(\tau)\ k^n & \text{if } \epsilon \le k \le k_c, \\ 0 & \text{otherwise,} \end{cases} \tag{51}$$

where A is a normalization constant; the infrared and ultraviolet cutoffs ϵ and k_c are imposed in order to regularize the loop integrations (SF1). In a cosmological N-body simulation, they would correspond roughly to the inverse comoving box size and lattice spacing (or interparticle separation) respectively.

In the absence of the cutoffs, the spectrum (51) would be scale-free. The introduction of fixed (time-independent) cutoff scales ϵ and k_c in the linear power spectrum (51) breaks self-similarity, because they do not scale with the self-similarity variable kR_0. The extent to which one can take the limits $\epsilon \to 0$ and $k_c \to \infty$ will determine whether one recovers self-similar scaling for the statistical properties of the density field. Infrared divergences, regulated by ϵ, arise in individual diagrams when $n \le -1$, due to the divergence of the rms velocity field at large scales (Jain & Bertschinger 1996, SF1). These divergences are just a kinematical effect and cancel when the sum over diagrams is done, as a consequence of the Galilean invariance of the equations of motion (SF1).

Ultraviolet divergences, on the other hand, arise due to small-scale power, and become more severe as n increases. In fact, for $n \ge -1$, one-loop corrections to the power spectrum break self-similarity (SF2)

$$\mathcal{P}(kR_0) = \frac{(kR_0)^n}{2\pi\ \Gamma\left(\frac{n+3}{2}\right)} - \frac{61\ (kR_0)^{2n+3}}{315\pi(n+1)\ \Gamma^2\left(\frac{n+3}{2}\right)}\ \left(\frac{k}{k_c}\right)^\eta, \tag{52}$$

where $\eta = -(n+1)$ is an exponent which measures the deviation from self-similar scaling, and the self-similarity breaking factor becomes a logarithm when $n = -1$.

We have done a similar calculation for the "tadpole" diagram (B^{II}_{321} and B_{411}) contributions to the bispectrum and found that the same self-similarity breaking factors appear in this case. For the other contributions, the explicit calculation is not possible to do analytically, but it can be checked by numerical integration that the full one-loop bispectrum breaks self-similarity for $n \ge -1$. For equilateral configurations, this calculation can be summarized by the one-loop result for $n > -1$:

$$\mathcal{B}^{(1)}(kR_0, kR_0) = b_n\ (kR_0)^{3n+3} \left(\frac{k}{k_c}\right)^\eta, \tag{53}$$

with b_n a finite n-dependent constant factor and logarithmic terms breaking self-similarity

as $n \to -1$. This breaking of self-similar evolution, not seen in numerical simulations, is a feature of the perturbative approach; it comes from large loop momenta due to increasing small scale power as n increases. We therefore do not expect our results to be physical as $n \to -1$ from below. On the other hand, for $-3 < n < -1$, one-loop corrections to the bispectrum scale as $(kR_0)^{3n+3}$ and preserve self-similar evolution. In this case, as was already considered for the power spectrum in SF2, it is more convenient to regularize the individual one-loop bispectrum diagrams by using dimensional regularization (see Appendix A), which effectively takes the limits $\epsilon \to 0$ and $k_c \to \infty$. We now turn to the results of this calculation.

4. One-Loop Results: Entering the Non-Linear Regime

4.1. Bispectrum

We now consider one-loop corrections to the bispectrum for initial power-law spectra $P_{11}(k) \propto k^n$ with spectral index $-3 < n < -1$. In this case, the resulting bispectrum obeys self-similarity and, based on previous results for the power spectrum (SF2), the perturbative approach is expected to give a good description of the transition to the nonlinear regime. Due to statistical homogeneity and isotropy, the bispectrum $B(\mathbf{k}_1, \mathbf{k}_2, \tau)$ in the scaling regime ($\epsilon \ll k_i \ll k_c$) only depends on time, the quantities k_1, k_2, and the angle θ ($\hat{k}_1 \cdot \hat{k}_2 \equiv \cos\theta$). In order to display the analytic results, however, it is more convenient to trade the variable θ for the third side of the triangle, $k_3 = |\mathbf{k}_1 + \mathbf{k}_2|$. Let $B^{(1)}(\mathbf{k}_1, \mathbf{k}_2) \equiv A^3 a^6 \pi^3 \; b^{(1)}(k_1, k_2, k_3)$, with $\mathbf{k}_1 + \mathbf{k}_2 + \mathbf{k}_3 \equiv 0$. Then, using the results of Appendix A, and summing over diagrams according to the results in Section 3.1, the one-loop correction to the bispectrum for $n = -2$ reads:

$$
\begin{aligned}
b^{(1)}(k_1,k_2,k_3) \;=\; & -\frac{30279}{34496\,{k_1}^3} - \frac{2635\,{k_1}^2}{51744\,{k_2}^5} - \frac{37313\,k_1}{206976\,{k_2}^4} + \frac{38431}{68992\,k_1\,{k_2}^2} \\
& + \frac{233\,{k_1}^6}{8624\,{k_2}^4\,{k_3}^5} - \frac{16517\,{k_1}^5}{362208\,{k_2}^3\,{k_3}^5} + \frac{197\,{k_1}^4}{7392\,{k_2}^2\,{k_3}^5} - \frac{78691\,{k_1}^3}{275968\,k_2\,{k_3}^5} \\
& - \frac{23\,{k_1}^5}{103488\,{k_2}^4\,{k_3}^4} + \frac{9791\,{k_1}^4}{206976\,{k_2}^3\,{k_3}^4} + \frac{703\,{k_1}^3}{68992\,{k_2}^2\,{k_3}^4} + \frac{19867\,{k_1}^2}{206976\,k_2\,{k_3}^4} \\
& + \frac{5311\,{k_1}^2}{34496\,{k_2}^2\,{k_3}^3} + \frac{42983\,k_1}{362208\,k_2\,{k_3}^3} + \frac{131\,k_1}{3696\,{k_2}^2\,{k_3}^2} + \frac{28393}{19712\,k_1\,k_2\,k_3} \\
& + \frac{53973\,{k_1}^7}{1931776\,{k_2}^5\,{k_3}^5} + \frac{108685\,k_1\,k_2}{181104\,{k_3}^5} + \frac{59599\,{k_1}^3}{362208\,{k_2}^3\,{k_3}^3} \\
& + \text{permutations.}
\end{aligned}
\tag{54}
$$

A well-known approximation scheme that provides insight into the physics of the non-linear regime is the Zel'dovich approximation (ZA) (Zel'dovich 1970). We therefore also consider the perturbative expansion for the ZA dynamics (see Appendix B), and calculate one-loop corrections to the bispectrum and skewness factor as well (loop corrections to the bispectrum in the ZA have been recently considered for spectra with small scale cutoffs and spectral indices $n > -1$ by Bharadwaj (1996)). For the one-loop bispectrum, again for $n = -2$, we find:

$$\begin{aligned} b^{(1)}(k_1,k_2,k_3) \;=\; & -\frac{27}{128\,{k_1}^3} - \frac{9\,k_1}{256\,{k_2}^4} + \frac{27}{256\,k_1\,{k_2}^2} + \frac{2187\,{k_1}^7}{32768\,{k_2}^5\,{k_3}^5} \\ & + \frac{9\,{k_1}^6}{256\,{k_2}^4\,{k_3}^5} - \frac{2853\,{k_1}^5}{16384\,{k_2}^3\,{k_3}^5} - \frac{9\,{k_1}^4}{256\,{k_2}^2\,{k_3}^5} - \frac{1467\,{k_1}^3}{32768\,k_2\,{k_3}^5} \\ & + \frac{2493\,k_1\,k_2}{8192\,{k_3}^5} - \frac{3\,{k_1}^4}{256\,{k_2}^3\,{k_3}^4} + \frac{3\,{k_1}^2}{256\,k_2\,{k_3}^4} + \frac{4863\,{k_1}^3}{16384\,{k_2}^3\,{k_3}^3} \\ & + \frac{3\,{k_1}^2}{128\,{k_2}^2\,{k_3}^3} - \frac{237\,k_1}{8192\,k_2\,{k_3}^3} + \frac{11823}{16384\,k_1\,k_2\,k_3} + \text{permutations}. \end{aligned} \tag{55}$$

Using the one-loop power spectrum for $n = -2$ given in SF2 (see also Makino et al. (1992))

$$p^{(1)}(k) = \frac{55}{98\;k}, \tag{56}$$

where $P^{(1)}(k) \equiv A^2 a^4 \pi^3\; p^{(1)}(k)$, we can obtain the one-loop hierarchical amplitude $Q^{(1)}$ from Eq. (41). Since $Q^{(1)}$ depends on time, a convenient parametrization of the degree of nonlinear evolution which takes advantage of self-similarity is to write wave-vectors in terms of the correlation length R_0 defined in Eq. (29), which for scale-free initial power spectra and Gaussian smoothing gives

$$R_0^{n+3} \equiv 2\pi\; A\; a^2\; \Gamma\Big(\frac{n+3}{2}\Big). \tag{57}$$

Figures 5 and 6 show the resulting hierarchical amplitude Q (see Eq. (37)), for the exact dynamics (ED) and the Zel'dovich approximation (ZA) respectively. We see that for the ED one-loop corrections to Q are in general not negligible even for weakly nonlinear scales. When $k_1 R_0 \approx 1$, the contribution to the variance per logarithmic interval $\Delta(k) \equiv 4\pi k^3 P(k)$ becomes of order one, and we expect one-loop perturbation theory to break down, since the scales considered become comparable to the correlation length. It is interesting that at these

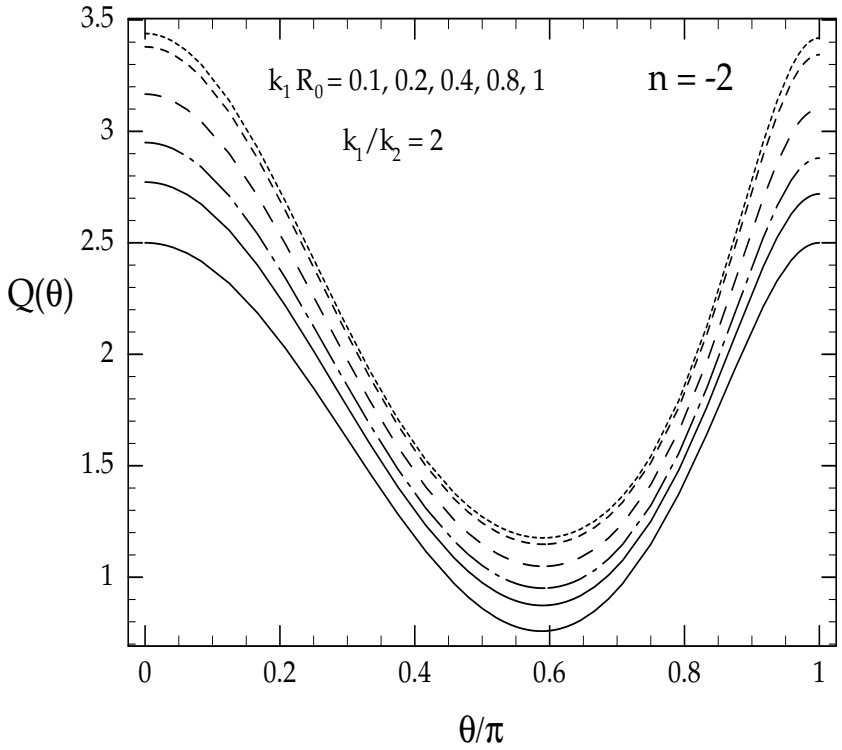

Fig. 5.— The hierarchical amplitude Q (see Eq. (37)) for triangle configurations ($k_1 = 1$, $k_2 = 0.5$; $\hat{k}_1 \cdot \hat{k}_2 \equiv \cos\theta$) as a function of the angle θ to one-loop. The lowest full curve shows Q at tree-level, whereas the subsequent curves correspond to different stages of non-linear evolution parameterized by the first side of the triangle in terms of the correlation length, $k_1 R_0 = 0.1, 0.2, 0.4, 0.8, 1$ (from bottom to top).

scales Eq. (37) *saturates*, that is, the one-loop quantities $B^{(1)}$ and $\Sigma^{(1)}$ dominate over the corresponding tree-level values and further time evolution does not change the amplitude Q, because $B^{(1)}$ and $\Sigma^{(1)}$ have the same scale and, by self-similarity, time-dependence. Note that for this initial spectrum, the one-loop correction *enhances* the configuration dependence of the tree-level bispectrum as the system evolves to the non-linear regime. This enhancement is stronger for the ZA, which is understandable in view of the tendency of this dynamics to produce highly anisotropic two-dimensional structures (pancakes). Note that the ZA underestimates the one-loop correction, in correspondence with the unsmoothed skewness (SF1) and power spectrum results (SF2).

Based on results from N-body simulations, it has been pointed out by Fry et al. (1993) (see also Fry et al. (1995)) that for $n = -1$ nonlinear evolution tends to "wash out" the configuration dependence of the bispectrum present at the largest scales (and given by

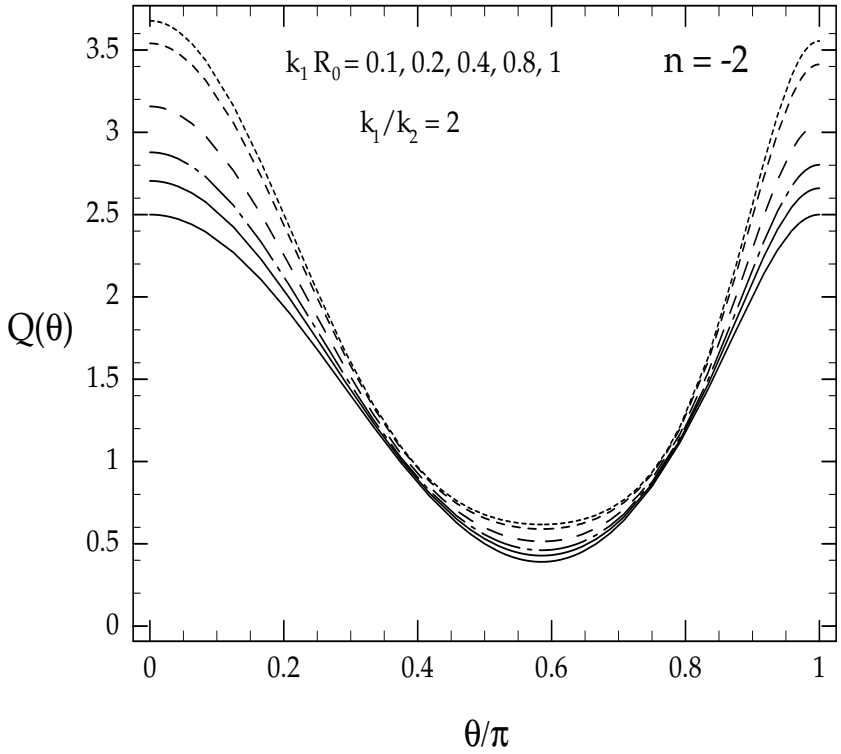

Fig. 6.— Same as Figure 5 for the Zel'dovich approximation.

tree-level perturbation theory), giving rise to the so-called hierarchical form $Q \approx const$ in the strongly non-linear regime. One-loop perturbation theory must predict this feature in order to be a good description of the transition to the nonlinear regime. To study this, we integrated numerically the one loop bispectrum for different spectral indices to understand the transition from the behavior at $n = -2$ to the $n = -1$ spectrum (for $n \neq -2$ the one-loop bispectrum can be represented in terms of hypergeometric functions of two variables (see Appendix A)). Figure 7 shows the result of such a calculation for the exact dynamics, in terms of the one-loop hierarchical amplitude $\tilde{Q}^{(1)}$ (see Eq. (41)) for spectral indices running from -1.6 to -1.3. Clearly one-loop perturbation theory predicts a change in behavior of the nonlinear evolution: for $n \lesssim -1.4$ the one-loop corrections *enhance* the configuration dependence of the bispectrum, whereas for $n \gtrsim -1.4$, they tend to cancel it, in qualitative agreement with numerical simulations. Note that this "critical index" $n_c \approx -1.4$ is the same spectral index at which one-loop corrections to the power spectrum vanish, marking the transition between faster and slower than linear growth of the variance of density field fluctuations (SF2) (see also Makino et al (1992), Łokas et al. (1995b), Bagla & Padmanabhan (1996)). Figure 8 shows that the same situation arises in the Zel'dovich approximation, which has $n_c \approx -1.75$. Figure 9 displays the one-loop correction to the power spectrum in both

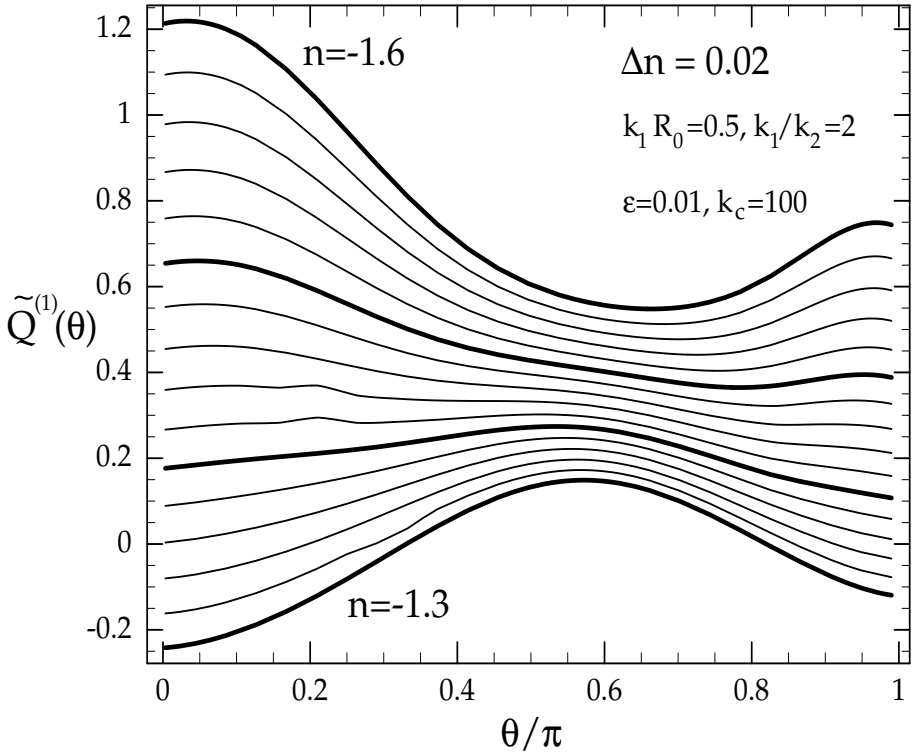

Fig. 7.— The one-loop hierarchical amplitude $\tilde{Q}^{(1)}$ (see Eq. (41)) for triangle configurations ($k_1 = 1$, $k_2 = 0.5$; $\hat{k}_1 \cdot \hat{k}_2 \equiv \cos\theta$) as a function of the angle θ for different spectral indices n. The spectral index runs from $n = -1.6$ (top full curve) to $n = -1.3$ (bottom full curve) in steps of $\Delta n = 0.02$. This shows the transition from positive to negative one-loop corrections as n is increased. The linear power spectrum in this figure is such that $\mathcal{P}_{11}(k) \equiv (kR_0)^n \exp[-(\epsilon/k)^4] \exp[-(k/k_c)^4]/[2\pi\Gamma[(n+3)/2]]$.

the exact dynamics (ED) and the Zel'dovich approximation (ZA) in terms of the function $\alpha(n)$ defined by

$$\mathcal{P}(kR_0) \equiv \frac{(kR_0)^n}{2\pi\Gamma[(n+3)/2]}\Big[1 + \alpha(n)\ (kR_0)^{n+3}\Big], \tag{58}$$

obtained by dimensional regularization in SF2. Figures 7, 8, and 9 clearly illustrate the special character of the critical index in both dynamics. Note that in Figures 7 and 8, the calculation is done by numerical integration and the linear power spectrum is not exactly scale-free, which can account for the very small shift in the critical index in these figures with respect to the exact scale-free case in Fig. 9.

The change in behavior of the one-loop corrections at $n \approx n_c$ can be understood in phys-

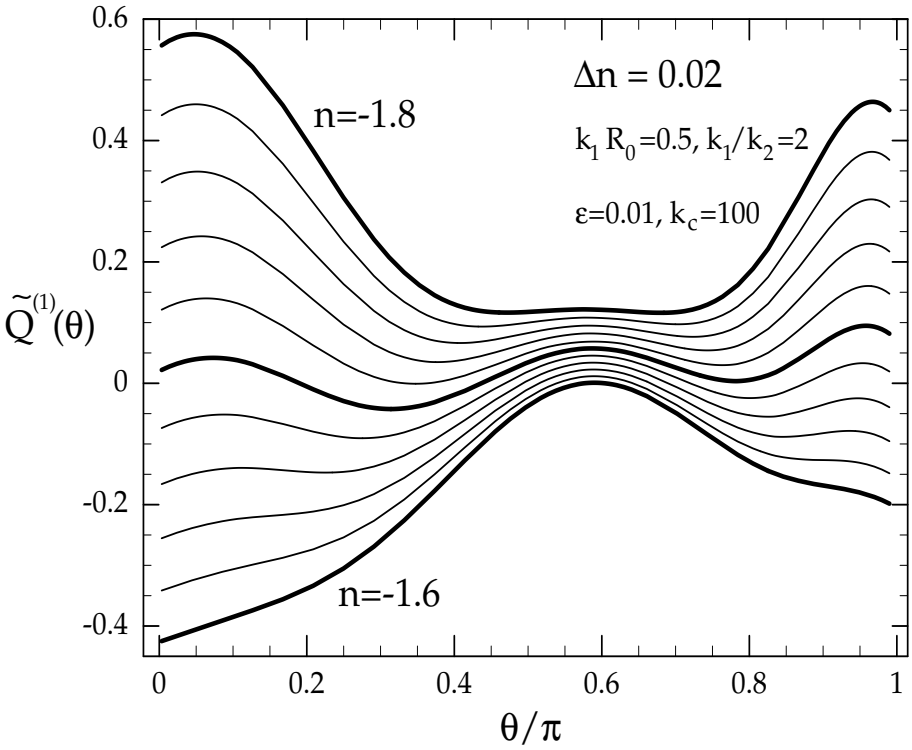

Fig. 8.— Same as Figure 7 for the Zel'dovich approximation.

ical terms as follows. As we increase n, the increase in small-scale power generates random motions which tend to prevent the collapse of high density regions (the "previrialization" effect (Davis & Peebles 1977, Evrard & Crone 1992, Łokas et al. 1995b, Peebles 1990). This is reflected in the sign change of one-loop corrections to the variance, which measures the growth of fluctuations. Another manifestation of this effect, which influences the shape of the bispectrum, is that random motions due to small-scale power cause structures to be less anisotropic and flows to have a smaller coherence length. This leads, upon ensemble averaging, to a cancellation of the configuration dependence in the hierarchical amplitude Q in Fourier space. A quantitative comparison of the predictions of one-loop perturbation theory with N-body simulations for the hierarchical amplitude Q is under way and is the subject of a forthcoming paper (Scoccimarro et al. 1996).

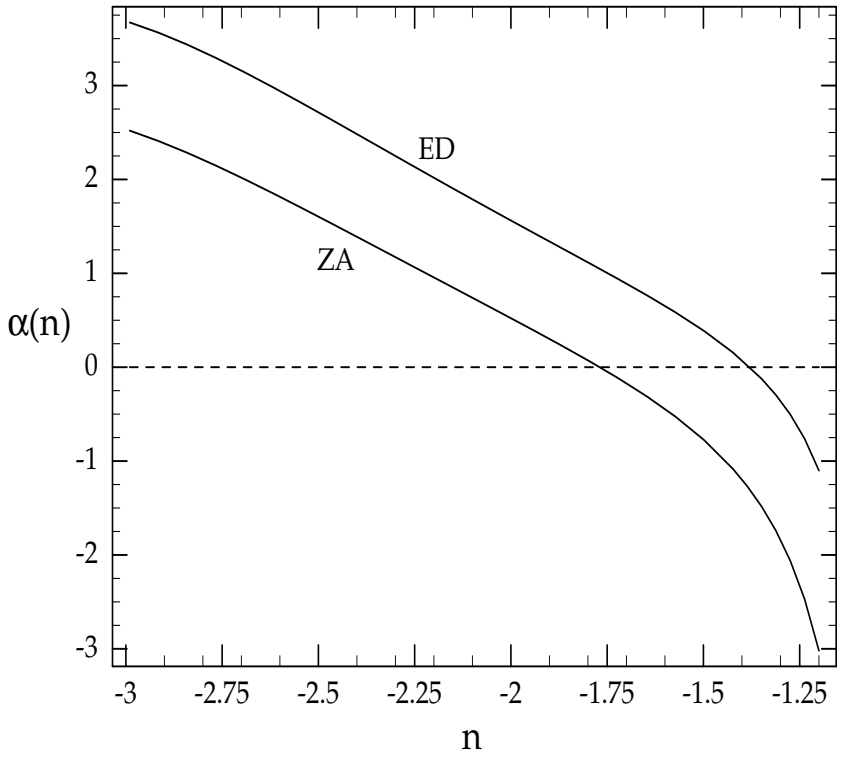

Fig. 9.— One-loop corrections to the power spectrum in the exact dynamics (ED) and Zel'dovich approximation (ZA) as a function of spectral index (see Eq. (58)).

4.2. Skewness: Comparison with Numerical Simulations

We now consider one-loop corrections to the skewness factor. Since tree-level one-point cumulants such as the skewness and kurtosis are given by the spherical collapse dynamics (Bernardeau 1992, Bernardeau 1994b), one-loop contributions contain the first corrections to the spherical model coming from tidal motions. Given the analytic results for the $n = -2$ bispectrum in the previous section, we can use Eq.(45) to integrate numerically the one-loop skewness for different window functions. For the exact dynamics, we obtain (see Eq. (43)):

$$S_3^{ED}(R) = \frac{3.86 + 9.97\ \sigma_{TH}^2(R)}{1 + 1.76\ \sigma_{TH}^2(R)}, \tag{59a}$$

$$\approx 3.86 + 3.18\ \sigma_{TH}^2(R), \tag{59b}$$

for top-hat smoothing, and

$$S_3^{ED}(R) = \frac{4.02 + 10.91\ \sigma_G^2(R)}{1 + 1.76\ \sigma_G^2(R)} \approx 4.02 + 3.83\ \sigma_G^2(R), \tag{60}$$

for Gaussian smoothing. For the Zel'dovich approximation we get:

$$S_3^{ZA}(R) = \frac{3 + 2.59\ \sigma_{TH}^2(R)}{1 + 0.59\ \sigma_{TH}^2(R)} \approx 3 + 0.82\ \sigma_{TH}^2(R), \tag{61}$$

for top-hat smoothing, and

$$S_3^{ZA}(R) = \frac{3.14 + 2.86\ \sigma_G^2(R)}{1 + 0.59\ \sigma_G^2(R)} \approx 3.14 + 1.00\ \sigma_G^2(R), \tag{62}$$

for Gaussian smoothing. We also computed one-loop corrections to the skewness in the Local Lagrangian approximation scheme discussed by Protogeros & Scherrer (1996). We obtain (see Appendix C):

$$S_3^{LLA}(R) = \frac{4 + 9.43\ \sigma_{TH}^2(R)}{1 + 1.39\ \sigma_{TH}^2(R)} \approx 4 + 3.87\ \sigma_{TH}^2(R), \tag{63}$$

for top-hat smoothing. Note that the results in Eqs. (59)-(4.2) are all for $n = -2$. A visual summary of the exact perturbative results is given in Fig. 10, where we compare to the

numerical simulations by Colombi et al (1996). These N-body simulations used a tree code (Hernquist, Bouchet & Suto 1991), with 64^3 particles in a cubic box with periodic boundary conditions. Symbols in Fig. 10 correspond to different output times: diamonds ($a = 2$), triangles ($a = 3.2$), and stars ($a = 5.2$). The estimated systematic uncertainties in these measurements of skewness is ± 0.1 in logarithmic scale, which is due to the uncertainty in the finite volume correction applied to the simulation data (see Colombi et al. (1996) and also Colombi et al. (1994), Hivon et al. (1995) for details). This correction, which is rather large because of the large-scale power present in the $n = -2$ spectrum, is more important when the correlation length becomes a non-negligible fraction of the box size (i.e., for larger a). For a given time output, the finite volume correction is more important for large scales. Note that only the two latest outputs in this figure have been corrected for finite volume effects; for the first output ($a = 2$) this correction should be negligible.

The two solid curves in Fig. 10 correspond to the predictions given in Eq. (59a) (bottom) and Eq. (59b) (top). The lower curve shows a saturation at values of $\sigma^2 \approx 1$ such that one-loop corrections in Eq. (59a) dominate over the tree-level contributions, similar to what happens with the hierarchical amplitude Q. This saturation value, however, is not in good agreement with the numerical simulation data, which is not surprising given that those scales are well into the non-linear regime. We note that the N-body results are systematically lower (although within the error bars) than the one-loop perturbative calculation in the weakly non-linear regime. In fact, as $\sigma^2 \to 0$ they approach asymptotically the tree-level value given in the Zel'dovich approximation. This is most likely an artifact coming from the fact that the simulation uses ZA initial conditions, which have not been erased by the relatively early output time at $a = 2$ (Baugh et al. 1995). Note that the dashed curves given by:

$$S_3(R) = \frac{3 + 9.97\ \sigma_{TH}^2(R)}{1 + 1.76\ \sigma_{TH}^2(R)}, \tag{64a}$$

$$\approx 3 + 4.69\ \sigma_{TH}^2(R), \tag{64b}$$

which are the tree-level value given by the ZA plus the one-loop correction in the exact dynamics, fit the numerical results better, suggesting that indeed transients from the ZA initial conditions are still present in the first output. It is interesting to note that the expansion for large scales given in Eq. (64b) seems to describe the transition to the non-linear regime better than Eq. (64a), which soon becomes dominated by one-loop corrections and driven to the saturation value. Overall, however, we see that one-loop perturbation theory agrees with the simulation within the error bars even on scales where $\sigma^2 \approx 1$, and therefore describes most of the transition from the tree-level result (valid in the limit $\sigma^2 \to 0$)

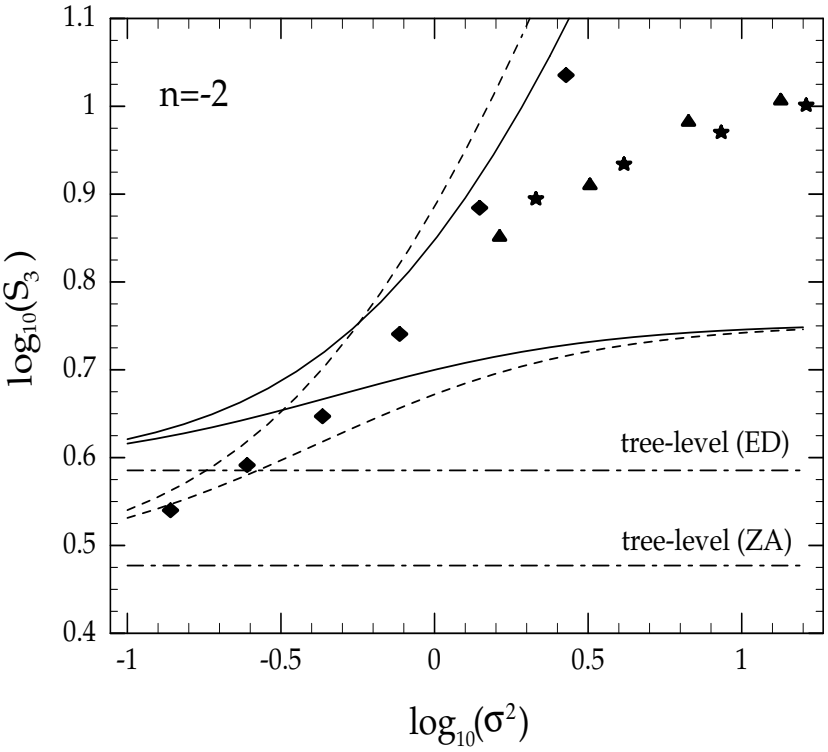

Fig. 10.— The skewness factor S_3 as a function of the variance of density fluctuations $\sigma^2(R)$ for spectral index $n = -2$. The symbols show the results from numerical simulations by Colombi et al. (1996) for top-hat smoothing. Different symbols correspond to different output times: diamonds ($a = 2$), triangles ($a = 3.2$), and stars ($a = 5.2$). Estimated error bars in these measurements are ± 0.1 (systematic) in logarithmic scale (Colombi et al. 1996). The solid curves correspond to the prediction for top-hat smoothing (TH) of exact one-loop perturbation theory (ED), Eqs. (59a) (bottom) and (59b) (top). Dashed lines denote the tree-level Zel'dovich approximation (ZA) plus one-loop ED, Eqs. (64a) (bottom) and (64b) (top). Dot-dashed lines correspond to tree-level values in ED and ZA.

to the nonlinear regime where S_3 approximately approaches a constant value, in agreement with the corresponding results for the power spectrum (SF2). A more detailed comparison, with more accurate N-body measurements, will be presented elsewhere.

The Zel'dovich approximation for S_3 clearly underestimates the numerical simulation and the exact dynamics perturbative results, in agreement with previous results for unsmoothed fields in SF1. Note that it also fails to describe properly the transition to the non-linear regime. The Local Lagrangian approximation (LLA) does reasonably well, although it overestimates the exact perturbative results; this is not surprising, given that it

has been "designed" to reproduce the tree-level one-point cumulants (Protogeros & Scherrer 1996). On the other hand, a phenomenological model recently proposed by Munshi & Padmanabhan (1996), which assumes the hierarchical ansatz (equivalent to a constant S_3), predicts $S_3 = 11.76$ for $-0.6 \lesssim \log_{10} \sigma^2 \lesssim 0.3$, in disagreement with the numerical simulation results, which do not support the hierarchical assumption in the transition to the non-linear regime.

It is interesting to note the importance of smoothing in the value of one-loop corrections by comparing the above results to the unsmoothed values found in SF1. For the exact dynamics, we obtained for unsmoothed fields

$$S_3^{ED} \approx 4.86 + 10.03\ \sigma^2, \tag{65}$$

for the $n = -2$ spectrum, where the corresponding result for the Zel'dovich approximation reads:

$$S_3^{ZA} \approx 4 + 4.69\ \sigma^2. \tag{66}$$

In each case, smoothing reduces the relative importance of the loop corrections. For the exact dynamics, one-loop corrections to the smoothed skewness begin to dominate over the tree-level contribution for $\sigma^2 \approx 1$, instead at $\sigma^2 \approx 1/2$ for unsmoothed fields.

Another interesting issue is the spectral dependence of the one-loop corrections to S_3. One-loop corrections to the variance and average two-point correlation function show a linear dependence on spectral index for $-3 < n < -1.5$ (SF2), and we conjecture that a similar behavior extends to S_3. For $n = -3$, smoothed and unsmoothed quantities coincide, because small-scale filtering does not affect statistical properties for a model with such extreme large-scale power (e.g., the variance is infrared-divergent). In this case, we have (SF1)

$$S_3(R) \approx \frac{34}{7} + 10\ \sigma_{TH}^2(R) \qquad (n = -3). \tag{67}$$

Taking into account the above results for $n = -2$, Eq. (59) and assuming linear behavior with n, we expect that for top-hat smoothing,

$$\begin{aligned} S_3(R,n) &\approx \frac{34}{7} - (n+3) + \sigma_{TH}^2(R)\ \Big[10 - 6.8\ (n+3)\Big] \\ &\approx \Big[\frac{34}{7} + 10\ \sigma_{TH}^2(R)\Big] - (n+3)\ \Big[1 + 6.8\ \sigma_{TH}^2(R)\Big]. \end{aligned} \tag{68}$$

In fact, as $n \to -1.6$, this ansatz leads to $S_3^{(1)} \to 0$, which is probably outside the region of validity of the linear extrapolation. For $n = -1$, for example, numerical simulations show that $S_3^{(1)} > 0$ (Colombi et al. 1996).

5. Conclusions

We have calculated one-loop corrections (non-linear corrections *beyond* leading order) to the bispectrum and skewness of the cosmological density field including smoothing effects, induced by gravitational evolution for Gaussian initial conditions and scale-free initial power spectra. These results extend previous calculations done at tree-level and allow us to probe the transition to the non-linear regime.

We have shown that the one-loop bispectrum follows a similar behavior as a function of spectral index as the one-loop power spectrum. For $n \lesssim -1.4$, one-loop corrections *increase* the configuration dependence of the bispectrum; for $n \gtrsim -1.4$, one-loop corrections tend to cancel the configuration dependence of the tree-level bispectrum, in agreement with $n = -1$ numerical simulations. Therefore, there is a "critical index" $n_c \approx -1.4$, similar to what happens in the case of the power spectrum, where one-loop corrections become negative at $n \gtrsim -1.4$ (SF2), indicating a slowing down of the growth of fluctuations (Łokas et al. 1995b). This increase in the configuration dependence of the bispectrum for $n < n_c$ is a prediction of one-loop perturbation theory that can be tested against numerical simulations. The configuration dependence of the bispectrum is due to the anisotropy of structures and flows in real space, and therefore has a direct physical meaning. In this respect, the one-loop bispectrum for the Zel'dovich approximation, which is well known to produce highly anisotropic structures (pancakes), shows a stronger configuration dependence, as expected. We interpret the change in behavior of the bispectrum as the spectral index increases as a result of the increased effect of small-scale power in the collapse of high density regions (the "previrialization" effect (Davis & Peebles 1977, Evrard & Crone 1992, Łokas et al. 1995b, Peebles 1990). The random motions due to small-scale power tend to slow down the collapse and disrupt coherent structures and flows on small scales, which is reflected in the one-loop corrections to the power spectrum and bispectrum respectively.

For spectral indices $n < -1$, self-similarity is retained at the one-loop level, and one can calculate loop corrections in the scaling regime by using the technique of dimensional regularization. We obtained explicit analytic results for the one-loop bispectrum for $n = -2$ initial conditions; this allowed us to calculate the skewness factor for top-hat and Gaussian smoothing. We then extended the results in SF1 to include local averaging of the fields; for $n = -2$, the smoothed one-loop correction is reduced by more than a factor of 2 from its

unsmoothed value, which shows the importance of smoothing in determining the value of one-loop corrections. The results for top-hat smoothing compare well with the corresponding measurements in numerical simulations, providing a description of most of the transition from the tree-level value at large scales ($\sigma \to 0$) to the non-linear regime where S_3 attains an approximate constant value in accord with expectations based on stable clustering.

The results presented in this work suggest future directions in which one can improve the current understanding of the transition to the non-linear regime. One obvious extension would be to consider spectral indices $n \geq -1$, to generalize the present results for arbitrary scale-free spectra. This would involve taking into account the effects of small-scale fluctuations on the evolution of large-scale modes in a way that absorbs the divergences that appear in the present formalism (renormalization), and therefore recovers self-similar evolution for statistical quantities such as the power spectrum and bispectrum. This would lead to a better understanding of the role of previrialization in determining the structure of the correlation functions on intermediate scales. We hope to come back to this point in the near future.

Since realistic power spectra are not scale-free, an important further step is to consider initial conditions such as those given by the cold dark matter (CDM) model and its variants. Since these models have effective spectral indices in the range $n_{eff} \approx -2$ to -1 over the scales of interest, we expect that they will show similar features to the ones we presented here. Nevertheless explicit calculations are required in order to assess the effect of one-loop corrections in the determination of bias from the configuration dependence of the bispectrum (Fry 1994). Similarly, recent claims by Jing & Börner (1996) that there is a discrepancy in the three-point function between tree-level perturbation theory and numerical simulations for CDM models, may be properly addressed by taking into account one-loop corrections. As we showed in this work, these can be non-negligible even on weakly non-linear scales, depending on the initial spectrum. Work is in progress on these issues (Scoccimarro et al. 1996).

There is clearly much more work to do to understand non-linear clustering in an expanding Universe. However, the interplay between perturbation theory and N-body simulations suggests that there are three distinct regimes that describe its most important statistical features. At the largest scales, tree-level perturbation theory is well established as providing a good description of the correlation functions and the $\sigma \to 0$ limit of the S_p parameters (Fry 1984, Bernardeau 1994). In the strongly non-linear regime, numerical simulations (Hamilton et al 1991, Peacock & Dodds 1994, Suto 1993, Jain et al. 1995, Colombi et al. 1996, Jain 1996) have shown reasonable agreement with the stable clustering hypothesis, although there are still large uncertainties due to limitations in dynamic range. In this regime, there

is as yet no compelling analytic model which makes predictions in good agreement with the numerical results, except probably for the two-point function (Sheth & Jain 1996). In particular, there is no understanding of the hierarchical structure of the S_p parameters, which seem to reach a plateau in the highly non-linear regime, $S_p \approx$ constant. Finally, the results presented in this work suggest that the third regime, the transition to the non-linear regime, with $\sigma \approx 1$, can be understood by one-loop perturbation theory for models without excessive small-scale power. This is clearly promising and deserves further investigation.

It's a pleasure to thank Josh Frieman, who has guided me in the research described in this work. I am indebted to Stephane Colombi for providing me with the results of his measurements in numerical simulations used in this paper and for many discussions on this subject. Special thanks are due to Jim Fry, with whom I cross-checked my numerical results on the one-loop bispectrum. I am also grateful to R. Cebral, D. Chung, L. Kadanoff, S. Meyer, and M. Turner for comments and discussions. Financial support by the DOE at Chicago and Fermilab and by NASA grant NAG5-2788 at Fermilab is particularly acknowledged.

A. Dimensional Regularization

To obtain the behavior of the one-loop N-point spectra for $n < -1$, one can use dimensional regularization (see e.g. Collins (1984)) to simplify considerably the calculations. Since we are interested in the limit $k_c \to \infty$, all the integrals run from 0 to ∞, and divergences are regulated by changing the dimensionality d of space: we set $d = 3 + \varepsilon$ and expand in $\varepsilon \ll 1$. For the bispectrum, we need the following one-loop three-point integral:

$$J(\nu_1, \nu_2, \nu_3) \equiv \int \frac{d^d\mathbf{q}}{(q^2)^{\nu_1}[(\mathbf{k_1} - \mathbf{q})^2]^{\nu_2}[(\mathbf{k_2} - \mathbf{q})^2]^{\nu_3}}. \tag{A1}$$

When one of the indices vanishes, e.g. $\nu_3 = 0$, this reduces to the standard formula for dimensional-regularized two-point integrals (Smirnov 1991):

$$J(\nu_1, \nu_2, 0) = \frac{\Gamma(d/2 - \nu_1)\Gamma(d/2 - \nu_2)\Gamma(\nu_1 + \nu_2 - d/2)}{\Gamma(\nu_1)\Gamma(\nu_2)\Gamma(d - \nu_1 - \nu_2)}\ \pi^{d/2}\ k_1^{d-2\nu_1-2\nu_2}. \tag{A2}$$

The integral $J(\nu_1, \nu_2, \nu_3)$ appears in triangle diagrams for massless particles in quantum field theory, and can be evaluated for arbitrary values of its parameters in terms of hypergeometric functions of two variables (Davydychev 1992). The result is:

$$
\begin{aligned}
J(\nu_1,\nu_2,\nu_3) &= \frac{\pi^{d/2}k_1^{d-2\nu_{123}}}{\Gamma(\nu_1)\Gamma(\nu_2)\Gamma(\nu_3)\Gamma(d-\nu_{123})}\times\Bigg(\Gamma(\nu_3)\Gamma(\nu_{123}-d/2)\\
&\quad\times \mathrm{F}_4(\nu_3,\nu_{123}-d/2;1+\nu_{23}-d/2,1+\nu_{13}-d/2;x,y)\\
&\quad\times\Gamma(d/2-\nu_{13})\Gamma(d/2-\nu_{23}) + y^{d/2-\nu_{13}}\Gamma(\nu_2)\Gamma(d/2-\nu_1)\\
&\quad\times \mathrm{F}_4(\nu_2,d/2-\nu_1;1+\nu_{23}-d/2,1-\nu_{13}+d/2;x,y)\\
&\quad\times\Gamma(\nu_{13}-d/2)\Gamma(d/2-\nu_{23}) + x^{d/2-\nu_{23}}\Gamma(\nu_1)\Gamma(d/2-\nu_2)\\
&\quad\times \mathrm{F}_4(\nu_1,d/2-\nu_2;1-\nu_{23}+d/2,1+\nu_{13}-d/2;x,y)\\
&\quad\times\Gamma(d/2-\nu_{13})\Gamma(\nu_{23}-d/2) + x^{d/2-\nu_{23}}y^{d/2-\nu_{13}}\Gamma(d/2-\nu_3)\\
&\quad\times \mathrm{F}_4(d-\nu_{123},d/2-\nu_3;1-\nu_{23}+d/2,1-\nu_{13}+d/2;x,y)\\
&\quad\times\Gamma(d-\nu_{123})\Gamma(\nu_{23}-d/2)\Gamma(\nu_{13}-d/2)\Bigg),
\end{aligned}
\tag{A3}
$$

where $\nu_{123}\equiv\nu_1+\nu_2+\nu_3$, $\nu_{ij}\equiv\nu_i+\nu_j$, $x\equiv(\mathbf{k}_2-\mathbf{k}_1)^2/k_1^2$, $y\equiv k_2^2/k_1^2$, and F_4 is Apell's hypergeometric function of two variables, with the series expansion:

$$
\mathrm{F}_4(a,b;c,d;x,y)=\sum_{i=0}^{\infty}\sum_{j=0}^{\infty}\frac{x^i y^j}{i!\;j!}\;\frac{(a)_{i+j}(b)_{i+j}}{(c)_i(d)_j},
\tag{A4}
$$

where $(a)_i\equiv\Gamma(a+i)/\Gamma(a)$ denotes the Pochhammer symbol. When the spectral index is $n=-2$, the hypergeometric functions reduce to polynomials in their variables due to the following useful property for $-a$ a positive integer:

$$
\mathrm{F}_4(a,b;c,d;x,y)=\sum_{i=0}^{-a}\sum_{j=0}^{-a-i}\frac{x^j y^i}{j!\;i!}\;\frac{(b)_{i+j}}{(c)_i(d)_j}\;\frac{(-1)^{i+j}(-a)!}{(-a-i-j)!}.
\tag{A5}
$$

When using Eq. (A3), divergences appear as poles in the gamma functions; these can be handled by the following expansion ($n=0,1,2,\ldots$ and $\varepsilon\to 0$):

$$
\Gamma(-n+\varepsilon)=\frac{(-1)^n}{n!}\left[\frac{1}{\varepsilon}+\psi(n+1)+\frac{\varepsilon}{2}\left(\frac{\pi^2}{3}+\psi^2(n+1)-\psi'(n+1)\right)+\mathcal{O}(\varepsilon^2)\right],
\tag{A6}
$$

where $\psi(x)\equiv d\ln\Gamma(x)/dx$ and

$$
\psi(n+1) = 1+\frac{1}{2}+\ldots+\frac{1}{n}-\gamma_e,
\tag{A7}
$$

$$\psi'(n+1) \;=\; \frac{\pi^2}{6} - \sum_{k=1}^{n} \frac{1}{k^2}, \tag{A8}$$

with $\psi(1) = -\gamma_e = -0.577216\ldots$ and $\psi'(1) = \pi^2/6$.

B. Zel'dovich Approximation

In this approximation (Zel'dovich 1970, Shandarin & Zel'dovich 1989), the motion of each particle is given by its initial Lagrangian displacement. In Eulerian space, this is equivalent to replacing the Poisson equation by the ansatz (Munshi & Starobinski 1994):

$$\mathbf{v}(\mathbf{x},\tau) = -\frac{2}{3\mathcal{H}(\tau)}\nabla\Phi(\mathbf{x},\tau), \tag{B1}$$

which is the relation between velocity and gravitational potential valid in linear theory. The important point about the ZA is that a small perturbation in Lagrangian fluid element paths carries a large amount of non-linear information about the corresponding Eulerian quantities, since the Lagrangian picture is intrinsically non-linear in the density field. This leads to non-zero Eulerian perturbation theory kernels at every order. The ZA works reasonably well as long as streamlines of flows do not cross each other. However, multistreaming develops at the location of pancakes, leading to the breakdown of ZA (Shandarin & Zel'dovich 1989). The equations of motion in Fourier space are:

$$\frac{\partial\tilde{\delta}(\mathbf{k},\tau)}{\partial\tau} + \tilde{\theta}(\mathbf{k},\tau) = -\int d^3k_1 \int d^3k_2 \delta_D(\mathbf{k}-\mathbf{k}_1-\mathbf{k}_2)\alpha(\mathbf{k},\mathbf{k}_1)\tilde{\theta}(\mathbf{k}_1,\tau)\tilde{\delta}(\mathbf{k}_2,\tau), \tag{B2}$$

$$\frac{\partial\tilde{\theta}(\mathbf{k},\tau)}{\partial\tau} - \frac{\mathcal{H}(\tau)}{2}\,\tilde{\theta}(\mathbf{k},\tau) = -\int d^3k_1 \int d^3k_2 \delta_D(\mathbf{k}-\mathbf{k}_1-\mathbf{k}_2)\beta(\mathbf{k},\mathbf{k}_1,\mathbf{k}_2)\tilde{\theta}(\mathbf{k}_1,\tau)\tilde{\theta}(\mathbf{k}_2,\tau)\ . \tag{B3}$$

These equations, together with the perturbative expansion (7), lead to the recursion relations ($n \geq 2$):

$$F_n^Z(\mathbf{q}_1,\ldots,\mathbf{q}_n) \;=\; \sum_{m=1}^{n-1} G_m^Z(\mathbf{q}_1,\ldots,\mathbf{q}_m)\Big[\frac{\alpha(\mathbf{k},\mathbf{k}_1)}{n}F_{n-m}^Z(\mathbf{q}_{m+1},\ldots,\mathbf{q}_n) + \frac{\beta(\mathbf{k},\mathbf{k}_1,\mathbf{k}_2)}{n(n-1)} \times G_{n-m}^Z(\mathbf{q}_{m+1},\ldots,\mathbf{q}_n)\Big], \tag{B4}$$

$$G_n^Z(\mathbf{q}_1,\ldots,\mathbf{q}_n) = \sum_{m=1}^{n-1} G_m^Z(\mathbf{q}_1,\ldots,\mathbf{q}_m)\frac{\beta(\mathbf{k},\mathbf{k}_1,\mathbf{k}_2)}{(n-1)}G_{n-m}^Z(\mathbf{q}_{m+1},\ldots,\mathbf{q}_n), \tag{B5}$$

After symmetrization, the density field kernel takes the simple form (Grinstein & Wise 1987):

$$F_n^{Z(s)}(\mathbf{q}_1,\ldots,\mathbf{q}_n) = \frac{1}{n!}\frac{(\mathbf{k}\cdot\mathbf{q}_1)}{q_1^2}\ldots\frac{(\mathbf{k}\cdot\mathbf{q}_n)}{q_n^2}. \tag{B6}$$

Using Eq. (B6) for $n = 2$ and (44), one can can calculate the skewness at tree-level for different window functions. For top-hat smoothing, the result is (Bernardeau 1994)

$$S_3^{(0)} = 4 - (n+3), \tag{B7}$$

whereas for Gaussian smoothing, using the methods described by Łokas et al. (1995), we obtain:

$$\begin{aligned} S_3^{(0)} &= 4\ {}_2\mathrm{F}_1\Big(\frac{n+3}{2},\frac{n+3}{2},\frac{3}{2},\frac{1}{4}\Big) - (n+3)\ {}_2\mathrm{F}_1\Big(\frac{n+5}{2},\frac{n+3}{2},\frac{5}{2},\frac{1}{4}\Big) \\ &\quad + \frac{(n+3)^2}{30}\ {}_2\mathrm{F}_1\Big(\frac{n+5}{2},\frac{n+5}{2},\frac{7}{2},\frac{1}{4}\Big), \end{aligned} \tag{B8}$$

where ${}_2\mathrm{F}_1$ denotes a hypergeometric function. More explicitly, for Gaussian smoothing, $S_3^{(0)} = 3.14,\ 2.80,\ 2.51,\ 2.26,\ 2.04$ for $n = -2, -1.5, -1, -0.5, 0$ respectively.

C. Local Lagrangian Approximation

In this approximation (Protogeros & Scherrer 1996), the final density at a Lagrangian point $\mathbf{q}$ at time τ is assumed to be a function only of the initial density at the same Lagrangian point and time τ:

$$\eta(\mathbf{q},\tau) \equiv \frac{\eta_0(\mathbf{q})}{[1 - a(\tau)\ \delta_0(\mathbf{q})/\alpha]^\alpha}, \tag{C1}$$

where $\eta \equiv 1+\delta$, with $\delta_0(\mathbf{q}) \equiv \delta(\mathbf{q},\tau_0)$ and τ_0 is the initial time. The constant α takes the value $\alpha = 1$ for the planar approximation (which becomes exact for one-dimensional collapse), whereas $\alpha = 3$ corresponds to spherical collapse in the Zel'dovich approximation. Local

Lagrangian approximations at the level of the equations of motion for fluid elements have been considered recently by Hui & Bertschinger (1996). In this work we restrict ourselves to the case $\alpha = 3/2$, which, although it has no particular physical meaning, can be shown to closely approximate the hierarchical amplitudes S_p of tree-level perturbation theory for the exact dynamics (Bernardeau 1992). Upon normalization of the probability distribution function for δ, the local Lagrangian approximation in this case reads:

$$\eta(\mathbf{q},\tau) \equiv \frac{\left\langle [1 - 2\ \delta_1(\mathbf{q},\tau)/3]^{3/2} \right\rangle_{lag}}{[1 - 2\ \delta_1(\mathbf{q},\tau)/3]^{3/2}}, \tag{C2}$$

where $<>_{lag}$ denotes ensemble averaging in Lagrangian space, and $\delta_1(\mathbf{q},\tau)$ corresponds to the evolution of the density contrast in linear perturbation theory. The S_p parameters are defined as ($p > 2$)

$$S_p \equiv \frac{< \delta^p >}{< \delta^2 >^{p-1}}, \tag{C3}$$

where the angular brackets correspond to Eulerian ensemble averages. For powers of η we have (Protogeros & Scherrer 1996)

$$< \eta^m > = < \eta^{m-1} >_{lag} . \tag{C4}$$

Given that, for Gaussian initial conditions, $< \delta_1^m > = (m-1)!!\ \sigma^m$ for m even and zero otherwise, one has everything needed to compute Eq. (C3) for unsmoothed density fields. The effects of top-hat smoothing for power-law power spectra can be included by the implicit mapping (Bernardeau 1994b, Protogeros & Scherrer 1996)

$$\eta_s = f[\delta_1\ \eta_s^{-(n+3)/6}], \tag{C5}$$

where $f(x) \equiv (1 - 2x/3)^{-3/2}$ denotes the unsmoothed mapping. We are particularly interested in $n = -2$, for which Eq. (C5) yields:

$$\eta_s = z^{-6}(\delta_1) < z^6(\delta_1) >_{lag} , \tag{C6}$$

where $z(\delta_1)$ denotes the appropriate solution to the quartic equation $z^4 = 1 - 2\delta_1 z/3$. Using Eqs. (C3) and (C4), we obtain for the skewness and kurtosis factors

$$S_3(R) = \frac{4 + 509/54\ \sigma_{TH}^2(R)}{1 + 25/18\ \sigma_{TH}^2(R)} \approx 4 + \frac{209}{54}\ \sigma_{TH}^2(R) \approx 4 + 3.87\ \sigma_{TH}^2(R), \tag{C7}$$

$$\begin{aligned} S_4(R) &= \frac{269/9 + 53661191/373248\ \sigma_{TH}^2(R)}{1 + 25/12\ \sigma_{TH}^2(R)} \approx \frac{269}{9} + \frac{30419591}{373248}\ \sigma_{TH}^2(R) \\ &\approx 29.88 + 81.49\ \sigma_{TH}^2(R). \end{aligned} \tag{C8}$$

REFERENCES

Bagla, J.S., & Padmanabhan, T. 1996, preprint, astro-ph/9605202

Baugh, C. M. & Efstathiou, G. 1994, MNRAS, 270, 183

Baugh, C. M., Gaztañaga, E., & Efstathiou, G. 1995, MNRAS 274, 1049

Bernardeau, F. 1992, ApJ, 392, 1

Bernardeau, F. 1994, ApJ, 433, 1

Bernardeau, F. 1994b, A & A 291, 697

Bernardeau, F. 1996, to appear in Proc. XXXI Moriond Meeting "Dark Matter in Cosmology, Quantum Measurements and Experimental Gravitation", astro-ph/9607004

Bertschinger, E. 1992, in New Insights into the Universe, ed. Martinez, V. J., Portilla, M., & Saez, D. (Berlin: Springer-Verlag) 65

Bharadwaj, S. 1996, preprint, astro-ph/9606121

Bouchet, F. R., & Hernquist, L. 1996, ApJ, 400 ,25

Bouchet, F. R. 1996, in CXXXII Enrico Fermi School on Dark Matter in the Universe, astro-ph/9603013

Collins, J. C., *Renormalization*, (Cambridge: Cambridge University Press)

Colombi, S., Bouchet, F. R., & Schaeffer, R. 1994, A & A, 281, 301

Colombi, S., Bouchet, F. R., & Hernquist, L. 1996, ApJ, 465, 14

Davis, M. & Peebles, P. J. E. 1977, ApJS, 34, 25

Davydychev, A. I. 1992, J Phys A, 25, 5587

Efstathiou, G., Frenk, C. S., White, S. D. M., & Davis, M. 1988, MNRAS, 235, 715

Evrard A. E. & Crone M. M. 1992, ApJ, 394, L1

Fry, J. N. 1984, ApJ, 279, 499

Fry, J. N. 1994, Phys. Rev. Lett., 73, 215

Fry, J. N., & Gaztañaga, E. 1993, ApJ, 413, 447

Fry, J. N., Melott, A. M. & Shandarin, S. F. 1993, ApJ, 412, 504

Fry, J. N., Melott, A. M. & Shandarin, S. F. 1995, MNRAS, 274, 745

Fry, J. N., & Seldner, M. 1982, ApJ, 259, 474

Gaztañaga, E. & Baugh, C. M. 1995, MNRAS, 273, L1

Goroff, M. H., Grinstein, B., Rey, S.-J., & Wise, M. B. 1986, ApJ, 311, 6

Grinstein, B., & Wise, M. B. 1987, ApJ, 320, 448

Hamilton, A. J. S., Kumar, P., Lu, E., & Matthews, A. 1991, ApJ , 374, L1

Hernquist, L., Bouchet, F. R. & Suto, Y. 1991, ApJS , 75, 231

Hivon, E., Bouchet, F. R., Colombi S., & Juszkiewicz, R. 1995, A & A , 298, 643

Hui, L. & Bertschinger, E. 1996, preprint, astro-ph/9508114

Jain, B. 1996, ApJ, preprint, astro-ph/9605192

Jain, B. & Bertschinger, E. 1994, ApJ, 431, 495

Jain, B. & Bertschinger, E. 1996, ApJ, 456, 43

Jain, B., Mo, H. J., & White, S. D. M. 1995, MNRAS, 276, L25

Jing, Y. P. & Börner, G. 1996, A & A, in press, astro-ph/9606122

Juszkiewicz, R. 1981, MNRAS, 197, 931

Juszkiewicz, R., Bouchet, F. R., & Colombi, S. 1993, ApJ, 412, L9

Juszkiewicz, R., Sonoda, D. H., & Barrow, J. D. 1984, MNRAS, 209, 139

Juszkiewicz, R., & Bouchet, F. R. 1996, in Proc. XXX Moriond Meeting: Clustering in the Universe, astro-ph/9602134

Juszkiewicz, R., Weinberg, D. H., Amsterdamski, P., Chodorowski, M. & Bouchet, F. R. 1995, ApJ, 442, 39

Łokas, E. L., Juszkiewicz, R., Weinberg, D. H. & Bouchet, F. R. 1995, MNRAS, 274, 730

Łokas, E. L., Juszkiewicz, R., Bouchet, F. R., & Hivon, E. 1996, ApJ, 467, 1

Lucchin, F., Matarrese, S., Melott, A. L., & Moscardini, L. 1994, ApJ, 422, 430

Makino, N., Sasaki, M., & and Suto, Y. 1992, Phys. Rev. D, 46, 585

Matsubara, T. 1994, ApJ, 434, L43

Munshi,D., & Padmanabhan, T. 1996, preprint, astro-ph/9606170

Munshi,D., & Starobinsky, A. A. 1994, ApJ, 428, 433

Peacock, J. A. & Dodds, S. J. 1994, MNRAS, 267, 1020

Peebles, P. J. E. 1974, A&A, 32, 391

Peebles, P. J. E. 1980, *The Large-Scale Structure of the Universe*, Princeton University Press

Peebles, P. J. E. 1900, ApJ, 365, 27

Peebles, P. J. E. & Groth, E. J. 1976, A&A, 53, 131

Protogeros, Z. A. M. & Scherrer, R. J. 1996, preprint, astro-ph/9603155

Sahni V. & Coles, P. 1996, Physics Reports, 262, 1

Scoccimarro, R. & Frieman, J. 1996, ApJS, 105, 37 (SF1)

Scoccimarro, R. & Frieman, J. 1996b, ApJ, 472, in press (SF2)

Scoccimarro, R., Colombi, S., Fry, J.N., Frieman, J., Hivon, E. & Melott, A. 1996, in preparation

Sheth, R. K., & Jain B., preprint, astro-ph/9602103

Shandarin, S. F., & Zel'dovich, Ya. B. 1989, Rev. Mod. Phys, 61, 185

Smirnov, V. A. 1991, *Renormalization and Asymptotic Expansions*, Birkhäuser Verlag, Berlin

Suto, Y. 1993, Prog. Theor. Phys., 90, 1173

Vishniac, E. T. 1983, MNRAS, 203, 345

Wise, M. B. 1988, in *The Early Universe*, W.G. Unruh and G. W. Semenoff (eds.), D. Reidel Publishing Company

Zel'dovich, Ya. B. 1965, Adv. Astron. Ap.,3, 241

Zel'dovich, Ya. B. 1970, A & A, 5, 84